Mean field theory for strongly coupled systems: Holographic approach

Supalert Sukrakarn, Taewon Yuk and Sang-Jin Sin ⓘD

Department of Physics, Hanyang University,
Seoul 04763, South Korea

E-mail: supalertee@gmail.com, tae1yuk@gmail.com, sangjin.sin@gmail.com

ABSTRACT: In this paper, we develop the holographic mean field theory for strongly interacting fermion systems. We investigate various types of the symmetry-breakings and their effect on the spectral function. We found analytic expressions of fermion Green's functions in the probe-limit for all types of tensor order parameter fields. We classified the spectral shapes and singularity types from the analytic Green's function. We calculated the fermions spectral function in the full backreacted background and then compared it with the analytic results to show the reliability of analytic results in the probe limit. The fact that all the main features of the spectral features in the current condensed matter physics including gaps of s-,p- waves, nodal rings and nodal shells, the flat band of dimension 1,2,3, can be obtained in the absence of the lattice as consequences of the order and symmetry breaking pattern, is a pleasant surprise.

Contents

1 Introduction

Study on strongly interacting system has been the frontier of physics for more than half century. It has been the continuous source of motivation for a new theoretical framework. Along this line, the gravity dual picture [1–6] has been suggested as a new paradigm to understand strange metals [7, 8] and quantum critical points (QCP) [9–11] of strongly coupled systems. A few experimental data were also compared with the theory showing agreements, especially in quark gluon plasma [12], in clean graphene [13–17] and surface of topological insulators [18, 19].

On the other hand, QCP itself is a phenomena at zero temperature taking a measure zero sector of the phase diagram. Therefore for the theory to be compared with experiment, it is essential to consider the symmetry broken phases as well as the unbroken phase in the neighborhood the QCP. Such symmetry breaking is an essential step for new collective phenomena because a phenomenon associated with many-body collective phenomena is possible only when we have an order that leads to a gap which protect the new ground state from the excitations causing disorder. Otherwise, we will only have Fermi Liquid. While gap calculation is usually

a consequence of a mean-field theory, which seeks the value of the condensation corresponding to the certain fermion bilinear, its validity is limited to weakly interacting cases. Therefore a dream for theorists is to develop a mean field theory which is valid for the strongly interacting system maintaining the spirit of Landau-Ginzburg and Wilson.

The strongly coupled systems share many similarities with the gravity system in the sense that both have an unreasonable speed of equilibration: the Plankian dissipation near the QCP is very similar to the exponentially fast scrambling power [20, 21] of black hole horizon. Therefore, it is not surprising to expect a mean-field theory for a strongly interacting system based on the gravity dual description. While it is hard to find the exact gravity dual of a given system, it is reasonable to assume the presence of approximate dual theory for a strongly interacting system. It can serve as a representative theory for the purpose of studying various types of the gaps and condensations as well as the singularity types of the Green functions for the strongly interacting systems.

Notice that in the holographic superconductor theory [22, 23], the gap calculation was exemplified by considering scalar-vector-gravity theory, which is an important ingredient of the holographic mean field theory (MFT). However, the heart of the MFT is to study the gap creation and the fermion spectrum together, which has not yet been done systematically for different types of condensations. Furthermore, because the holographic theory as a continuum field theory does not encode the condensed matter system's detail, it is useful to study all possible types of interactions together and classify their spectral behavior to match the physical system's spectral pattern. In ref. [24] we put forwarded a step to such direction by considering all possible couplings of the bulk fermion bilinears with the various tensorial fields representing the different condensations in holographic set-up, which is analogue of the femion bilinear coupled to the Hubbard-Stratonovich field in the usual mean field theory.

In our previous work [24], the fermion spectral function (SF) [25–28] of each broken symmetry phase was calculated and classified. Subsequently, we realized that [29] the gapless mode in the scalar coupling is the AdS analogue of the surface mode of topological insulator whose topological stability might be related to amazing stability of the Fermi Liquid. The holographic mean field theory has universal structure so that it has the power to accommodate various different phenomena in the same fashion. Just as the superconductivity is described by the condensation of itinerant electrons $\Delta_S \sim cc$, one may also expect a new quantum ground state of manybody coming from the condensation of the itinerant-localized electrons with spin. Such many Kondo phenomena would be also described by considering the scalar condensation $\Delta_K \sim f^\dagger c$ if the mean field theory works for strongly interacting case like Kondo system. Recently, we realized such idea in the holographic set-up [30] by finding that the Kondo condensation Δ_K produces a gap, which was also observed experimentally [30].

However, the ref. [24] has several limitations: i) it is completely numerical so that it is hard to characterize the singularity types of the spectral functions. ii) the back reaction was not taken care of. iii) it was confined to the AdS_4 so that it is not possible to discuss the Weyl semi-metal spectrum from the beginning. In this paper, we will find the analytic expressions of the Green's function for all tensor types of symmetry breaking in the probe limit. Three aspects of the spectral function will be emphasized: i) gap/gapless, ii) presence/absence of flat bands of various types, iii) presence/absence of split Dirac cones. An especially interesting coupling

turned out to be the scalar type coupling, which can give both gapped and gapless spectrums depending on the sign of the coupling, which can never be possible in flat space theory.

From the analytic expressions, we noticed that most of the Green functions have branch-cut singularities, but some of them have poles, and we can now understand why various different types of flat bands exist. The definition of the non-Fermi Liquid is the vanishing of the quasi-particle weight assuming that the Green function has a pole type singularity. In our holographic mean field theory, it turns out that the generic form of the fermion propagator does not have pole singularity but has the branch cut singularity. That is, the fluid appearing in our theory is generically non-Fermi Liquid. Interestingly, in some cases, such behavior can happen even after order parameter is turned on. However, for a few types of the order parameter, the pole type singularity appears. Typically, it happens when the flat band appears.

At this moment, our analytic expressions are only for the case where order parameter fields are alternatively quantized where only the leading term is nonvanishing in the pure AdS background. In standard quantization where only the subleading term of the matter field is nonvanishing, we still have not find exact Green functions even in the probe limit. To back up this limitation, we performed and presented the numerical analysis to find fully backreacted solutions of the antisymmetric 2-tensor field, which is the most important and complicated case. We calculated the spectral function of the fermions based on such backreacted solution, and compared with the analytic result of the probe limit. In case the singularity is of pole type, we observed a detailed agreement between the approximate analytic result and the fully back-reacted numerical result, which suggests the stability of the Green function with the pole type singularity. In contrast, for the propagators with branch-cut type singularity, the detail of the spectrum is relatively vulnerable to the deformation by back-reaction, although qualitative similarity remains.

Before we go ahead to formulate our theory, we notice that our analytic work uses pure $\mathrm{AdS}_{4(5)}$ background but the zero temperature limit with broken symmetry usually involves a nontrivial backreaction. So, we want to explain what kind of approximation we are doing by using pure AdS. Also, one might ask that there is a formulation of semi-holography [31–33] which is based on $\mathrm{AdS}_2 \times \mathrm{R}^2$, which seems to reproduce the Fermi Liquid as well as non-Fermi Liquid. Here we want to describe how our theory and the semi-holography fit into a big picture.

We start by pointing out that the semi-holography is about the IR fixed point near zero temperature, the metallic $\mathrm{AdS}_2 \times \mathrm{R}^2$. Such geometry describes one of the quantum critical points (QCP). Although one can still introduce finite temperature or symmetry breaking there, the energy scale should be hierarchically closer to zero temperature than ours because AdS_2 is relevant only in that limit. See figure 1(a,b). It seems to us that the $\mathrm{AdS}_2 \times \mathrm{R}^2$ geometry is more relevant to the heavy fermion physics where QCP is exposed (not hidden by the ordered region) and Fermi Liquid is close to the QCP as well as the non-Fermi Liquid in that phase diagram.

Our aim is not such extreme zero temperature limit. The prototype model of our theory is the holographic superconductivity where the back reacted geometry is a hairy black hole that has a regular horizon and the near boundary region is still AdS_4. Notice that it has been argued that the zero temperature limit of holographic superconductor (HSC) is also Lifshitz geometry [34], but the main property of HSC, can be discussed in terms of the hairy black hole, which is a simple deformation of the RN geometry apart from near zero temperature
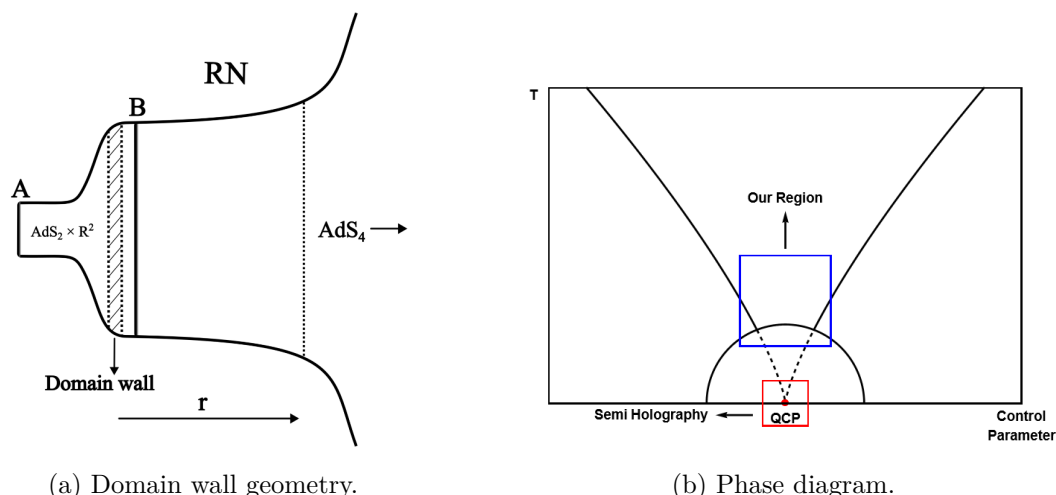
(a) Domain wall geometry.   (b) Phase diagram.

Figure 1. (a) Hierarchical difference of the temperatures: AdS_2 temperature vs AdS_4 temperature. The position A and B are the positions of the 'would be horizons' of AdS_2 and AdS_4, respectively. (b) Our theory is effective field theory in the regime of the blue box, while Semi-holography is that of red box near QCP at $T = 0$. For heavy fermion cases, the dome is not hiding the QCP.

regime. Therefore we want to avoid such near zero temperature regime. Also, notice that the High T_c superconducting material's phase diagram shows that the QCP is usually hidden in the superconducting dome. See figure 1(a). The upper region of the dome must be associated with the hairy black hole phase with the horizon and asymptotic AdS_4 intact. For us, the most interesting temperature regime is not the regime near QCP itself but the regime where the transition between the ordered dome and strange metal is available. Remember that the strange metal is not just a low energy phenomenon. It continues from the temperature, which is bigger than the order parameter, up to the melting temperature of the lattice.

In the figure 1(b), we denoted our interested regime by a box for the case of the HSC. Our target is the analogue of such regime for various scalar/vector/tensor order parameters. Most importantly, the pure AdS we used for analytic calculation is NOT the approximation of the zero temperature IR fixed point geometry, but that of a hairy black hole. The basic intuition is that, since we are choosing the horizon data such that we get the zero source term (or zero condensation) at the boundary and we read off the physics from the boundary behavior of the bulk fields, we assumed that the qualitative features of the Green function remain the same whether we use pure AdS or hairy black hole as far as the asymptotic geometry is remained as AdS_4. Of course, this should be confirmed by the detailed numerical calculation. In section 5 where we considered the fully back reaction, the considered geometry is the analogue of the hairy black hole, not the analogue of the IR fixed point geometry, and in some of the most interesting cases where the Green functions have pole type singularities, we found that the result of the probe analysis is rather robust under the correction of the back reaction.

The spectral features found in this paper by symmetry breaking includes gaps of s-,p-, types and nodal rings and nodal shells and the flat band of various dimensions. d-wave gap is not discussed here but it can be obtained from the symmetric rank two tensors [35–37]. The fact that these features of spectral features in the current condensed matter physics

can be obtained in the absence of the lattice as consequences of the order and symmetry breaking, are pleasant surprises. It is also interesting to notice that some of these features which were found in the weakly interacting topological system are also found in holographic system suggests that they should also be found in the strongly interacting systems.

The rest of this paper goes as following. In section 2, we give a short description of formalism of the holographic mean field theory and fermion Green function calculation. In section 3, we calculate Green's function analytically and draw spectral function for all types of the Lorentz symmetry breaking. In section 4, we draw spectral functions and discuss features of them. In section 5, we do extensive numerical calculation to find the fully back-reacted order parameter and metric and use them to calculate the fermion spectral function again to support the probe limit analytic results. In section 6, we discuss and conclude.

2 Holographic mean field theory with symmetry breaking

Our holographic mean field theory has four components: first, Bulk fermions ψ, which are dual to the boundary fermions with strong interactions. Second, order parameter fields Φ^I describe the condensations of fermion bilinear, which is the analog of the Hubbard-Statonovich field of the usual mean-field theory. Third, gravity describes the interactions between electrons, and finally, the gauge field should be included to describe the density or chemical potential of the fermions. In this work, we do not include the vector for the analytic work, but we can do it when we work numerically. For simplicity, we assume that they can be described by local fields in bulk, not in the boundary because we should allow the strongly interacting system in the boundary to be described by nonlocal field theory. The total action is given by [28]

$$S_{\text{total}} = S_\psi + S_{\text{bdy}} + S_{g,\Phi} + S_{\text{int}}, \tag{2.1}$$

$$S_\psi = \int d^5x \sum_{j=1}^2 \sqrt{-g}\, \bar{\psi}^{(j)} \left(\frac{1}{2}(\overrightarrow{\slashed{D}} - \overleftarrow{\slashed{D}}) - m^{(j)} \right) \psi^{(j)}, \tag{2.2}$$

$$S_{g,\Phi} = \int d^5x \sqrt{-g} \left(R - 2\Lambda + |D_M \Phi_I|^2 - m_\Phi^2 |\Phi|^2 \right), \tag{2.3}$$

$$S_{\text{bdy}} = \frac{i}{2} \int_{\text{bdy}} d^4x \sqrt{-h} \left(\bar{\psi}^{(1)} \psi^{(1)} \pm \bar{\psi}^{(2)} \psi^{(2)} \right), \tag{2.4}$$

$$S_{\text{int}} = \int d^5x \sqrt{-g} \left(\bar{\psi}^{(1)} \Phi \cdot \Gamma \psi^{(2)} + h.c \right). \tag{2.5}$$

where $\slashed{D} = \Gamma^M(\partial_M + \frac{1}{4}\omega_{M\alpha\beta}\Gamma^{\alpha\beta})$, $\omega_{M\alpha\beta}$ is the spin connection, $\Phi \cdot \Gamma = \Gamma^{\underline{\mu_1\mu_2\cdots\mu_I}}\Phi_{\underline{\mu_1\mu_2\cdots\mu_I}}$. Φ^I is the order parameter field which couples with bilinear spinor in the bulk, leading to the symmetry breaking under the presence of the source or its condensation. Additionally, we will turn on just one component of field Φ to calculate the spectral function. The gamma matrix convention and the geometry are chosen and given as follows,

$$\Gamma^{\underline{t}} = \sigma_1 \otimes i\sigma_2, \quad \Gamma^{\underline{x}} = \sigma_1 \otimes \sigma_1, \qquad \Gamma^{\underline{y}} = \sigma_1 \otimes \sigma_3, \quad \Gamma^{\underline{z}} = \sigma_2 \otimes \sigma_0, \quad \Gamma^{\underline{u}} = \sigma_3 \otimes \sigma_0 \quad (2.6)$$

$$ds^2 = \frac{1}{u^2}\left(dt^2 + \sum_{i=1}^3 d\vec{x}_i^{\,2} + du^2 \right), \quad f(u) = 1, \qquad h = gg^{uu}, \qquad u_h = \infty, \qquad (2.7)$$

where the underlined indices represent tangent space ones. Under this convention, the boundary locates at $u = 0$.

Notice that in AdS$_5$, including two-flavors of fermions is mandatory because holography projects out half of the fermion degrees of freedom while we need a full 4 component spinor in the 4 dimensional boundary. On the other hand, in AdS$_4$, considering one flavor is still allowed since the boundary is of 2+1 dimension where spinors are of two components.

We will analytically determine and analyze the fermions' Green's function in the presence of an order parameter field. So, we consider the absence of gauge field for simplicity. Furthermore, we will begin our analysis in the probe limit and later we will eventually calculate the spectral function in the full back-reacted background. We will compare it with the probe limit analytic results to check the reliability of the latter.

2.1 Variational analysis and boundary actions

In this section, we will perform the variational analysis in detail to show the boundary fermions in different quantization choices. The standard-standard (SS) and standard-alternative (SA) quantization can be distinguished by the sign of the boundary action (2.4). We first simplify the action by introducing $\zeta^{(j)}$,

$$\psi^{(j)} = (-gg^{uu})^{-1/4}\zeta^{(j)}e^{-i\omega t+ik_x x+ik_y y+ik_z z}. \tag{2.8}$$

Then, the variation of bulk fermions action (2.2), after the equation of motion is imposed can be written as a boundary term given below.

$$\delta S_{bulk} = \frac{i}{2}\sum_{i=1}^{2}\int d^4x\Big[\bar{\zeta}_-^{(i)}\delta\zeta_+^{(i)} - \bar{\zeta}_+^{(i)}\delta\zeta_-^{(i)} - \delta\bar{\zeta}_-^{(i)}\zeta_+^{(i)} + \delta\bar{\zeta}_+^{(i)}\zeta_-^{(i)}\Big]. \tag{2.9}$$

If we add the variation of boundary action with sign $\pm$ (2.4) depending on SS and SA quantization respectively, the variation of total action is given by

$$\delta S_{tot}^{(SS)} = \frac{i}{2}\int_{bdy} d^4x\Big(\bar{\zeta}_-^{(1)}\delta\zeta_+^{(1)} + \delta\bar{\zeta}_+^{(1)}\zeta_-^{(1)} + \bar{\zeta}_-^{(2)}\delta\zeta_+^{(2)} + \delta\bar{\zeta}_+^{(2)}\zeta_-^{(2)}\Big), \tag{2.10}$$

$$\delta S_{tot}^{(SA)} = \frac{i}{2}\int_{bdy} d^4x\Big(\bar{\zeta}_-^{(1)}\delta\zeta_+^{(1)} + \delta\bar{\zeta}_+^{(1)}\zeta_-^{(1)} - \bar{\zeta}_+^{(2)}\delta\zeta_-^{(2)} - \delta\zeta_-^{(2)}\zeta_+^{(2)}\Big). \tag{2.11}$$

From this expression, we see what are chosen as independent degree of freedom to makes the variation of total action zero. We call such independent fermions as the source fermions. We define a 4 component spinor ξ's by

$$\xi_S^{(SS)} := (\zeta_+^{(1)}, \zeta_+^{(2)}), \quad \text{and} \quad \xi_C^{(SS)} := (\zeta_-^{(1)}, \zeta_-^{(2)}), \tag{2.12}$$

as the boundary spinors for SS-quantization. The indices S, C in ξ_S and ξ_C are adopted since they correspond to the source and condensation terms. The ξ_C's supposed to be determined by ξ_S's. Similarly, for the SA-quantization we define

$$\xi_S^{(SA)} := (\zeta_+^{(1)}, \zeta_-^{(2)}), \quad \text{and} \quad \xi_C^{(SA)} := (\zeta_-^{(1)}, \zeta_+^{(2)}). \tag{2.13}$$

One should remember that all $\zeta_\pm$ are two component spinors while ξ's are 4 component ones. The extension $\xi(u)$ of these fermions to the bulk of the AdS can also be considered by the original $\zeta(u)$'s whose boundary values were used above as ζ, so that

$$\xi(u) = u^{m_s}\xi_S + u^{m_c}\xi_C + \cdots . \tag{2.14}$$

We can now rewrite the on-shell effective action as

$$S_{\text{tot}}^{(SS)} = \frac{1}{2}\int_{\text{bdy}} d^4x\Big(\xi_S^{(SS)\dagger}(-\sigma_0 \otimes \sigma_2)\xi_C^{(SS)} + h.c\Big), \tag{2.15}$$

$$S_{\text{tot}}^{(SA)} = \frac{1}{2}\int_{\text{bdy}} d^4x\Big(\xi_S^{(SA)\dagger}(-\sigma_3 \otimes \sigma_2)\xi_C^{(SA)} + h.c\Big). \tag{2.16}$$

2.2 Green's function

We can determine the boundary Green's functions from the effective actions (2.15)–(2.16) and the definition of source and condensation fermions. Since we have 4 components of $\xi(u)$, there must be 4 independent solutions $\boldsymbol{\Psi}_i(u)$ which can span the space of spinor solutions. Our $\xi(u)$ with prescribed boundary value should be a linear combination of these, so that

$$\xi(u) = \sum_i c^i \boldsymbol{\Psi}_i(u). \tag{2.17}$$

By taking the a-th component of this equation, we have $\xi^a(u) = \Psi_i^a(u)c^i$, which can be written as a matrix equation $\xi(u) = \boldsymbol{\Psi}(u)\mathbf{c}$. Here $\Psi_i^a(u)$ is the a-th component of i-th solution and we considered $\xi(u)$ and $\mathbf{c}$ as column matrices. By expanding the matrix $\boldsymbol{\Psi}(u)$ near the boundary,

$$\boldsymbol{\Psi}(u) = u^{m_s}\mathbb{S} + u^{m_c}\mathbb{C} + \cdots \tag{2.18}$$

We now can write the source and condensation fermions depending on the quantization choice as follows,

$$\xi_S^{(\mathbb{Q})} = \mathbb{S}^{(\mathbb{Q})}\mathbf{c}, \quad \xi_C^{(\mathbb{Q})} = \mathbb{C}^{(\mathbb{Q})}\mathbf{c}. \tag{2.19}$$

where $\mathbb{Q}$ stands for quantization choice. From eqs. (2.15)–(2.16) and using (2.19),

$$S_{\text{total}}^{(\mathbb{Q})}\Big|_{\text{bdy}} = \frac{1}{2}\int_{\text{bdy}} d^4x\Big(\xi_S^\dagger \Gamma_{\text{bdy}}\xi_C + h.c\Big)^{(\mathbb{Q})}, \tag{2.20}$$

$$= \frac{1}{2}\int_{\text{bdy}} d^4x(\xi_S^\dagger \Gamma_{\text{bdy}}\mathbb{C}\mathbb{S}^{-1}\xi_S + h.c)^{(\mathbb{Q})}, \tag{2.21}$$

$$= \frac{1}{2}\int_{\text{bdy}} d^4x(\xi_S^\dagger \mathbb{G}\xi_S + h.c)^{(\mathbb{Q})}. \tag{2.22}$$

the boundary Green's function can be defined as follow

$$\mathbb{G}^{(SS)} = -(\sigma_0 \otimes \sigma_2)\mathbb{C}\mathbb{S}^{-1}, \tag{2.23}$$

$$\mathbb{G}^{(SA)} = -(\sigma_3 \otimes \sigma_2)\mathbb{C}\mathbb{S}^{-1}. \tag{2.24}$$

Notice that the definition of Green's function remains valid even for the zero bulk fermion mass. Consequently, as far as we can extract the leading-order terms of the bulk fermions

near the boundary, Green's function calculation remains solvable. This is helpful because, in the zero fermion mass, we will be able to obtain Green's function analytically for all Lorentz symmetry-breaking interactions with the proper choice of scaling dimension of the order parameter field. The term suitable here refers to choosing scaling dimensions for the source term, in which any u-dependence in the interacting term will be eliminated after fully expressing the vierbein and spin connection. This ensures the results remain u-independent at the interaction terms and allows solvable Dirac equations.

3 Analytic Green's function of fermions in symmetry broken phases

We now consider zero bulk mass fermions with a holographic order parameter having only the leading term by setting $\langle \mathcal{O}_\Phi \rangle = 0$. This is so-called alternative quantization of the Φ. This setup allows us to derive Green's function for all types of Lorentz symmetry-breaking analytically. We have already performed numerical calculations to study the case of non-zero fermion bulk mass and the case with condensation in previous works [38–40]. From the expressions of Γ in (2.7) and

$$\Gamma^{tx} = \sigma_0 \otimes \sigma_3, \qquad \Gamma^{ty} = \sigma_0 \otimes -\sigma_1, \qquad \Gamma^{tz} = \sigma_3 \otimes -\sigma_2, \tag{3.1}$$

$$\Gamma^{xy} = \sigma_0 \otimes -i\sigma_2, \qquad \Gamma^{xz} = \sigma_3 \otimes i\sigma_1, \qquad \Gamma^{yz} = \sigma_3 \otimes i\sigma_3, \tag{3.2}$$

$$\Gamma^{ut} = i\sigma_2 \otimes i\sigma_2, \qquad \Gamma^{ux} = i\sigma_2 \otimes \sigma_1. \qquad \Gamma^{uy} = i\sigma_2 \otimes \sigma_3, \qquad \Gamma^{uz} = \sigma_1 \otimes -i\sigma_0 \tag{3.3}$$

our gamma matrices can be expressed in the following decomposed form:

$$\Gamma^{\underline{\mu}} = \begin{pmatrix} 0 & \gamma^{\underline{\mu}} \\ \gamma^{\underline{\mu}*} & 0 \end{pmatrix}, \quad \Gamma^{\underline{\mu\nu}} = \begin{pmatrix} \gamma^{\underline{\mu\nu}} & 0 \\ 0 & \gamma^{\underline{\mu\nu}*} \end{pmatrix}, \Gamma^{\underline{\mu}u} = \begin{pmatrix} 0 & \gamma^{\underline{\mu}} \\ -\gamma^{\underline{\mu}*} & 0 \end{pmatrix}, \tag{3.4}$$

where $\gamma^{\underline{\mu}} = (i\sigma_2, \sigma_1, \sigma_3, -i\slashed{k})$ with $\mu = t, x, y, z$ and $\gamma^{\underline{\mu\nu}} = \gamma^{\underline{\mu}}\gamma^{\underline{\nu}}$. The complex conjugation appears due to Γ^z's being pure imaginary. In AdS$_4$, this decomposition is still valid with $\mu = t, x, y$, because apart from Γ^5, all gamma matrices are real. So that the complex conjugate disappears in AdS$_4$. Such decomposition will be utilized for analytic solutions.

Classification of interaction types. Since the boundary represents the physical world, we will classify the interaction type from the boundary point of view;

- 2 types of scalar: $\mathbb{1}$, Γ^u(radial scalar).

- 2 types of vector: Γ^μ(polar vector), $\Gamma^{\mu u}$(radial vector).

- 1 type of tensor: $\Gamma^{\mu\nu}$(polar antisymmetric 2-tensor).

Although B^u and $B^{\mu u}$ are component of vector and tensor, respectively, they are scalar and vector from the boundary point of view,

3.1 Scalar: $\mathcal{L}_{\text{int}} = i\Phi(\bar{\psi}^{(2)}\psi^{(1)} + h.c)$

For scalar interaction, the solvable solution can be obtained by choosing

$$\Phi(u) = M_0 u + \underbrace{M}_{=0} u^3 \,; \qquad m_\Phi^2 = -3$$

SS case. The bulk equations of motion are given by

$$[\partial_u - M_0(\sigma_1 \otimes \sigma_0)]\xi_S^{(SS)} + i(\sigma_0 \otimes \gamma^{\underline{\mu}}k_\mu)\xi_C^{(SS)} = 0, \tag{3.5}$$

$$[\partial_u + M_0(\sigma_1 \otimes \sigma_0)]\xi_C^{(SS)} - i(\sigma_0 \otimes \gamma^{\underline{\mu}*}k_\mu)\xi_S^{(SS)} = 0, \tag{3.6}$$

due to the simple commutation relation between $(\sigma_0 \otimes \gamma^{\underline{\mu}*}k_\mu)$, and its conjugate, one can get the simple fully diagonalized decoupled equations [29], which reads

$$(\partial_u^2 - M_0^2 - \boldsymbol{k}^2 + \omega^2)\xi_{S,C}^{(SS)} = 0, \tag{3.7}$$

The solutions are well-known and decay exponentially since the growing terms are removed by imposing in-falling boundary condition (BC). As a result, the asymptotic solutions near the AdS boundary located at $u = 0$ are given by

$$\xi_S^{(SS)}|_{\text{bdy}} \simeq [\mathbb{S}_0(k) + \mathbb{S}_1(k)u + \cdots]\mathbf{c} \ , \ \ \xi_C^{(SS)}|_{\text{bdy}} \simeq [\mathbb{C}_0(k) + \mathbb{C}_1(k)u + \cdots]\mathbf{c}, \tag{3.8}$$

where $\mathbb{S}_n, \mathbb{C}_n$ are u-independent but momentum dependent 4×4 matrices. But apart from the leading term $\mathbb{S}_0(k), \mathbb{C}_0(k)$, they will not contribute to the boundary Green's function. Therefore we will write them simply as $\mathbb{S}(k), \mathbb{C}(k)$ by deleting the index 0. Since ξ_S and ξ_C are solved independently, one can plug-in one of the solution on the Dirac equations to find the relation between them [27, 28]. The condensation term is determined by the source term by solving the Dirac equation and it is given as follows:

$$\mathbb{C}(k) = i\frac{\sigma_0 \otimes \gamma^{\underline{\mu}*}k_\mu}{\boldsymbol{k}^2 - \omega^2}[\mathcal{T}(k) - M_0(\sigma_1 \otimes \sigma_0)]\mathbb{S}(k), \tag{3.9}$$

where we define the matrix $\mathcal{T} = \mathbb{S}_1\mathbb{S}_0^{-1}$. For the scalar interaction, it is given by

$$\mathcal{T}(k) = -\sqrt{\boldsymbol{k}^2 - \omega^2 + M_0^2} \ \mathbb{1}_{4\times 4}, \tag{3.10}$$

From the definition of boundary Green's function (2.24), one gets 4 by 4 retarded Green's function as follows,

$$\mathbb{G}(k)_R = -\frac{\Gamma^{\underline{t}}}{\boldsymbol{k}^2 - \omega^2}(\sigma_1 \otimes \gamma^{\underline{\mu}*}k_\mu)[\mathcal{T}(k) - M_0(\sigma_1 \otimes \sigma_0)], \tag{3.11}$$

$$= \frac{1}{\boldsymbol{k}^2 - \omega^2}\Big[\sqrt{\boldsymbol{k}^2 - \omega^2 + M_0^2} \ \sigma_0 + M_0 \ \sigma_1\Big] \otimes \mathbb{K}. \tag{3.12}$$

where

$$\boldsymbol{k}^2 = k_x^2 + k_y^2 + k_z^2, \quad \mathbb{K} := (\gamma^{\underline{t}}\gamma^{\underline{\mu}}k_\mu)^T = \begin{pmatrix} k_x + \omega & -k_y + ik_z \\ -k_y - ik_z & -k_x + \omega \end{pmatrix} \tag{3.13}$$

It is important to note that $\text{Tr}\,\mathbb{K} = 2\omega$, which will play a consistent role in our subsequent calculations. We will discuss the trace result of the Green's functions in the next section.

SA case. The bulk equations of motion are given by

$$\partial_u\xi_S^{(SA)} - (\sigma_2 \otimes \sigma_0)[\Gamma^{\underline{\mu}*}k_\mu + iM_0]\xi_C^{(SA)} = 0, \tag{3.14}$$

$$\partial_u\xi_C^{(SA)} + (\sigma_2 \otimes \sigma_0)[\Gamma^{\underline{\mu}}k_\mu - iM_0]\xi_S^{(SA)} = 0, \tag{3.15}$$

similar to the SS case, one can decouple above equations which again yields (3.7)–(3.8). Plugging the asymptotic solution into (3.14), we get

$$\mathbb{C}(k) = [\Gamma^{\underline{\mu}*} k_\mu + iM_0]^{-1}(\sigma_2 \otimes \sigma_0)\mathcal{T}(k)\mathbb{S}(k), \tag{3.16}$$

following the definition of Green's function, and the $\mathcal{T}(k)$ given in (3.10), one can get the general form of it as follows.

$$\mathbb{G}(k_\mu)_R = -(\sigma_3 \otimes \sigma_2)[\Gamma^{\underline{\mu}*} k_\mu + iM_0]^{-1}(\sigma_2 \otimes \sigma_0)\mathcal{T}(k) \tag{3.17}$$

$$= \frac{1}{\sqrt{\boldsymbol{k}^2 - \omega^2 + M_0^2}}\Big[\sigma_0 \otimes \mathbb{K} + M_0\ \sigma_1 \otimes \sigma_1\Big]. \tag{3.18}$$

where $\boldsymbol{k}$ and $\mathbb{K}$ are defined in (3.1). One can see that the Green's function contains off-diagonal terms, which are absent in intra-flavor interaction case. Moreover, calculating AA (alternative-alternative) or AS(alternative-standard) quantization cases yields the results with the propagator replaced by the complex conjugation.

3.2   Radial scalar: $\boldsymbol{\mathcal{L}_{\text{int}} = B_u(\bar{\psi}^{(2)}\Gamma^u \psi^{(1)} + h.c)}$

The solvable solution can be obtained by choosing

$$B_u(u) = b + \underbrace{b_u^{(2)}}_{=0} u^2\,; \qquad m_{B_u}^2 = 0,$$

where b is the constant measuring the symmetry breaking strength.

SS case. The bulk equations of motion are given by

$$[\partial_u - i(\sigma_1 \otimes \sigma_0)b]\xi_S^{(SS)} + i(\sigma_0 \otimes \gamma^{\underline{\mu}} k_\mu)\xi_C^{(SS)} = 0, \tag{3.19}$$

$$[\partial_u - i(\sigma_1 \otimes \sigma_0)b]\xi_C^{(SS)} - i(\sigma_0 \otimes \gamma^{\underline{\mu}*} k_\mu)\xi_S^{(SS)} = 0. \tag{3.20}$$

Decoupled differential equations (DEs) are given by

$$[\partial_u^2 - 2ib(\sigma_1 \otimes \sigma_0)\partial_u + (\boldsymbol{k}^2 - \omega^2 + b^2)]\xi_{S,C}^{SS} = 0, \tag{3.21}$$

Then, we can diagonalize the system by using the similarity transformation $\mathcal{P}$ defined by the eigenvectors matrix of $\sigma_1 \otimes \sigma_0$ which yields

$$[\partial_u^2 - 2ib\partial_u + (\boldsymbol{k}^2 - \omega^2 + b^2)]\mathcal{P}^{-1}\xi_{S,C}^{SS} = 0, \tag{3.22}$$

This yields the solution of the exponential form even after mapping the solution back by the inverse similarity transformation. So, overall, nothing new for B_u case. We can still write the Green's function as follows:

$$\mathbb{C}(k) = i\frac{(\sigma_0 \otimes \gamma^{\underline{\mu}*} k_\mu)}{\boldsymbol{k}^2 - \omega^2}[\mathcal{T}(k) - i(\sigma_1 \otimes \sigma_0)b]\mathbb{S}(k), \tag{3.23}$$

The surprise of this interaction types is structure of $\mathcal{T}(k)$, which is given by

$$\mathcal{T}(k) = -\sqrt{\boldsymbol{k}^2 - \omega^2} + i(\sigma_1 \otimes \sigma_0)b, \tag{3.24}$$

So the Green's function reduces into the non-interacting case,

$$\mathbb{G}(k) = i(\sigma_0 \otimes \sigma_2)\frac{(\sigma_0 \otimes \gamma^{\underline{\mu}*}k_\mu)}{\sqrt{\boldsymbol{k}^2 - \omega^2}} = \frac{\sigma_0 \otimes \mathbb{K}}{\sqrt{\boldsymbol{k}^2 - \omega^2}}. \tag{3.25}$$

SA case. The bulk dirac equation is given by

$$\partial_u \xi_S^{SA} - [(\sigma_2 \otimes \sigma_0)\Gamma^{\underline{\mu}*}k_\mu + i(\sigma_1 \otimes \sigma_0)b]\xi_C^{SA} = 0,$$
$$\partial_u \xi_C^{SA} + [(\sigma_2 \otimes \sigma_0)\Gamma^{\underline{\mu}}k_\mu - i(\sigma_1 \otimes \sigma_0)b]\xi_S^{SA} = 0,$$

Since the product of $[(\sigma_2 \otimes \sigma_0)\Gamma^{\underline{\mu}}k_\mu + i(\sigma_1 \otimes \sigma_0)b]$ and its complex conjugation is a non-diagonal matrix, a similarity transformation is needed for the diagonalization, which yields

$$[\partial_u^2 + (b - i\sqrt{\boldsymbol{k}^2 - \omega^2})^2]P^{-1}\xi_\pm^{SA} = 0. \tag{3.26}$$

The fermion Green's functions for SS and SA quantization with B_u interactions are found to be the same. This discovery raises the question of why SS and SA lead to identical Green's functions despite the differences in their equations of motion. The answer lies in two critical factors that influence the structure of the Green's function. Firstly, it depends on the combination of gamma matrices present in the Dirac equation, which varies with the choice of quantization. Secondly, the solutions are affected by the proper in-falling boundary conditions (BC). As a result, despite the apparent difference in the initial appearance of the Dirac equations, the solutions surviving the BC end up with the same Green's function.

3.3 Polar vectors: $\mathcal{L}_{\mathbf{int}} = B_\mu(\bar{\psi}^{(2)}\Gamma^\mu\psi^{(1)} + h.c)$

The solvable solution can be obtained by choosing

$$B_\mu(u) = B_\mu^{(0)} + \underbrace{B_\mu^{(2)}}_{=0} u^2\,; \qquad m_{B_\mu}^2 = 0. \tag{3.27}$$

where $B_\mu^{(0)}$ is a vectors with a single nonzero component $b_{(t,i)}$ which is nothing other than a constant order parameter.

SS case. The bulk equations of motion are given by

$$\partial_u \xi_S^{(SS)} + i[\sigma_0 \otimes \gamma^{\underline{\mu}}k_\mu - \sigma_1 \otimes \gamma^{\underline{\mu}}B_\mu^{(0)}]\xi_C^{(SS)} = 0, \tag{3.28}$$
$$\partial_u \xi_C^{(SS)} - i[\sigma_0 \otimes \gamma^{\underline{\mu}*}k_\mu - \sigma_1 \otimes \gamma^{\underline{\mu}*}B_\mu^{(0)}]\xi_S^{(SS)} = 0, \tag{3.29}$$

Unlike the scalar case, polar vector type interactions cannot be decoupled simply in this basis. However, we can transform the equations to a suitable basis by a u-independent similarity transformation, $\mathcal{P}$, where

$$\mathcal{P}^{-1}\mathcal{B}^*\mathcal{B}\mathcal{P} = (\mathcal{K}_{\mu_-}^2\,\sigma_0 \oplus \mathcal{K}_{\mu_+}^2\,\sigma_0),$$

where $\mathcal{B} := [\tilde{\Gamma}^{\underline{\mu}}k_\mu - \sigma_1 \otimes \gamma^\mu B_\mu^{(0)}]$, and $\mathcal{K}_{\mu_\pm}^2 := \boldsymbol{k}_\perp^2 + (b_\mu \pm k_\mu)^2$. Under this transformation, we can get the decoupled equations,

$$[\partial_u^2 - (\mathcal{K}_{\mu_-}^2\,\sigma_0 \oplus \mathcal{K}_{\mu_+}^2\,\sigma_0)]\tilde{\xi}_{S,C}^{(SS)} = 0, \tag{3.30}$$

where $\tilde{\xi}_{S,C} = P^{-1}\xi_{S,C}$. We obtain simple solutions even after transforming the solutions back to the original basis, providing exponential decay. Consequently, we can express the asymptotic solution similar to scalar case (3.8). By substituting the solution into the (3.28), we obtain

$$\mathbb{C}(k) = i[\sigma_0 \otimes \gamma^{\underline{\mu}} k_\mu - \sigma_1 \otimes \gamma^{\underline{\mu}} B_\mu^{(0)}]^{-1} \mathcal{T}(k) \mathbb{S}(k), \tag{3.31}$$

Then, the Green's function is given by

$$\mathbb{G}(k) = -i(\sigma_0 \otimes \sigma_2)[\sigma_0 \otimes \gamma^{\underline{\mu}} k_\mu - \sigma_1 \otimes \gamma^{\underline{\mu}} B_\mu^{(0)}]^{-1} \mathcal{T}(k). \tag{3.32}$$

The Green's functions can be determined straightforwardly by plugging in $\mathcal{T}(k)$ into (3.32). Now let us calculate the explicit expression of the Green's function.

B_t/SS. By solving the Dirac equations, one gets

$$\mathcal{T}(k)_{B_t^{(0)}}^{(SS)} = -\frac{1}{2}\Big((\mathcal{K}_{t_-} + \mathcal{K}_{t_+})\mathbb{1}_{4\times 4} + (\mathcal{K}_{t_+} - \mathcal{K}_{t_-})\sigma_1 \otimes \sigma_0\Big), \tag{3.33}$$

where

$$\mathcal{K}_{t_\pm} = \sqrt{\boldsymbol{k}^2 - (b_t \pm \omega)^2} \quad \text{and} \quad b_t = B_t^{(0)}, \tag{3.34}$$

By plugging the above result into (3.32), we can get the Green's function:

$$\mathbb{G}(k)_{B_t^{(0)}}^{(SS)} = \frac{1}{2\mathcal{K}_{t_+}\mathcal{K}_{t_-}} \begin{pmatrix} g_{11} & g_{12} \\ g_{21} & g_{22} \end{pmatrix}, \tag{3.35}$$

$$\text{with} \quad g_{11} = g_{22} = \Big((\mathcal{K}_{t_-} - \mathcal{K}_{t_+})b_t\sigma_0 + (\mathcal{K}_{t_-} + \mathcal{K}_{t_+})\mathbb{K}\Big),$$

$$g_{12} = g_{21} = \Big((\mathcal{K}_{t_-} + \mathcal{K}_{t_+})b_t\sigma_0 + (\mathcal{K}_{t_-} - \mathcal{K}_{t_+})\mathbb{K}\Big). \tag{3.36}$$

B_x/SS. By follwing the same calculation of time-like case, one gets

$$\mathcal{T}(k)_{B_x^{(0)}}^{(SS)} = -\frac{1}{2}\Big((\mathcal{K}_{x_-} + \mathcal{K}_{x_+})\mathbb{1}_{4\times 4} + (\mathcal{K}_{x_-} - \mathcal{K}_{x_+})\sigma_1 \otimes \sigma_0\Big), \tag{3.37}$$

where

$$\mathcal{K}_{x_\pm} = \sqrt{(b_x \pm k_x)^2 + \boldsymbol{k}_\perp^2 - \omega^2}, \quad \boldsymbol{k}_\perp^2 = k_y^2 + k_z^2, \quad \text{and} \quad b_x = B_x^{(0)}, \tag{3.38}$$

By plugging the $\mathcal{T}(k)$ in the above result into (3.32), one gets

$$\mathbb{G}(k)_{B_x^{(0)}}^{(SS)} = \frac{1}{2\mathcal{K}_{x_+}\mathcal{K}_{x_-}} \begin{pmatrix} g_{11} & g_{12} \\ g_{21} & g_{22} \end{pmatrix}, \tag{3.39}$$

$$\text{with} \quad g_{11} = g_{22} = \Big((\mathcal{K}_{x_-} - \mathcal{K}_{x_+})b_x\sigma_3 + (\mathcal{K}_{x_-} + \mathcal{K}_{x_+})\mathbb{K}\Big),$$

$$g_{12} = g_{21} = -\Big((\mathcal{K}_{x_-} + \mathcal{K}_{x_+})b_x\sigma_3 + (\mathcal{K}_{x_-} - \mathcal{K}_{x_+})\mathbb{K}\Big). \tag{3.40}$$

One can see that the Green's function of polar vectors together with SS quantization contains branch-cut singularity by the presence of $\mathcal{K}_{\mu\pm}^{-1}$ as the denominator terms. The

singularity type does not change after tracing the Green's function matrix, which we will discuss in the next section.

After this case, we will no longer show the full expression of $\mathcal{T}(k)$, because it will become more complicated while lacking meaningful content. However, one can obtain the Green's function by following the same logic and calculations.

SA case. The bulk equations of motion are given by

$$(\partial_u - i\Gamma^{\underline{u}\mu}B^{(0)}_\mu)\xi^{(SA)}_S - (\sigma_2 \otimes \sigma_0)\Gamma^{\underline{\mu}*}k_\mu\xi^{(SA)}_C = 0, \tag{3.41}$$

$$(\partial_u + i\Gamma^{\underline{u}\mu*}B^{(0)}_\mu)\xi^{(SA)}_C + (\sigma_2 \otimes \sigma_0)\Gamma^{\underline{\mu}}k_\mu\xi^{(SA)}_S = 0, \tag{3.42}$$

In this case, the differential equations cannot be fully decoupled by similarity transformation. However, the DE is nothing but a linear Ordinary DE system. Similar to other cases, the solutions satisfying the infalling BCs exponential decay (3.8). We, therefore, substitute the solution back to the (3.41) and get the condensation in terms of the source:

$$\mathbb{C}(k) = \frac{\Gamma^{\underline{\mu}*}k_\mu}{\boldsymbol{k}^2 - \omega^2}(\sigma_2 \otimes \sigma_0)[\mathcal{T}(k) - i\Gamma^{\underline{u}\mu}B^{(0)}_\mu]\mathbb{S}(k), \tag{3.43}$$

Therefore, the algebraic Green's function for this case is given by

$$\mathbb{G}(k)_R = -\frac{\Gamma^{\underline{t}}}{\boldsymbol{k}^2 - \omega^2}\Gamma^{\underline{\mu}}k_\mu[\mathcal{T}(k) - i\Gamma^{\underline{u}\mu}B^{(0)}_\mu]. \tag{3.44}$$

$\boldsymbol{B_t}/\textbf{SA}.$ After getting $\mathcal{T}(k)$ by solving the Dirac equation, and plugging in (3.44), one can get

$$\mathbb{G}(k)^{(SA)}_{B^{(0)}_t} = \frac{1}{2b_t\boldsymbol{k^2}}\begin{pmatrix} g_{11} & g_{12} \\ g_{21} & g_{22} \end{pmatrix}, \tag{3.45}$$

$$\text{with} \quad g_{11} = g^*_{22} = \Big(\omega(\mathcal{K}_{t_-} - \mathcal{K}_{t_+}) + b_t(\mathcal{K}_{t_-} + \mathcal{K}_{t_+})\Big)\mathbb{K}$$

$$- \Big(b_t\omega(\mathcal{K}_{t_-} + \mathcal{K}_{t_+}) - \mathcal{E}(\mathcal{K}_{t_-} - \mathcal{K}_{t_+})\Big)\sigma_0,$$

$$g_{12} = g^*_{21} = i(k_x\sigma_1 + \sigma_0\gamma^{\underline{\mu}}k_\mu)(b^2_t - \mathcal{K}_{t_-}\mathcal{K}_{t_+} + \mathcal{E}). \tag{3.46}$$

where $\mathcal{K}_{t_\pm}, b_t$ are defined in (3.34), and $\mathcal{E} = \boldsymbol{k}^2 - \omega^2$. One can easily check that the pole type singularity $\boldsymbol{k}^{-2}$ will be canceled out after we take the trace of this Green's function. Since the cancellation of the pole makes the trace of the Green's function becomes non-singularity type Green's function. Therefore, the presence of singularities in the 4 by 4 expression of the Green's function does not guarantee the presence of singularity in spectral function.

$\boldsymbol{B_x}/\textbf{SA}.$ By the same calculation in the previous cases, the Green's function reads

$$\mathbb{G}(k)^{(SA)}_{B^{(0)}_x} = \frac{1}{2b_x(\boldsymbol{k}^2_\perp - \omega^2)}\begin{pmatrix} g_{11} & g_{12} \\ g_{21} & g_{22} \end{pmatrix}, \tag{3.47}$$

$$\text{with} \quad g_{11} = g^*_{22} = \Big(k_x(\mathcal{K}_{x_-} - \mathcal{K}_{x_+}) + b_x(\mathcal{K}_{x_-} + \mathcal{K}_{x_+})\Big)\mathbb{K}$$

$$- \Big(b_xk_x(\mathcal{K}_{x_-} + \mathcal{K}_{x_+}) + \mathcal{E}(\mathcal{K}_{x_-} - \mathcal{K}_{x_+})\Big)\sigma_3,$$

$$g_{12} = g^*_{21} = (k_x\sigma_2 - i\sigma_3\gamma^{\underline{\mu}}k_\mu)(b^2_x + \mathcal{K}_{x_-}\mathcal{K}_{x_+} - \mathcal{E}). \tag{3.48}$$

where $\mathcal{K}_{x\pm}, \boldsymbol{k}_\perp, b_x$ are defined in (3.38) and $\mathcal{E} = \boldsymbol{k}^2 - \omega^2$. In this case, the singularity $(\boldsymbol{k}_\perp^2 - \omega^2)^{-1}$ is not changed or canceled by the trace, so that the trace of the Green's function has pole type singularity. We will back to discuss the trace of these Green's functions in the next sections.

3.4 Radial vectors: $\mathcal{L}_{\text{int}} = B_{\mu u}(\bar{\psi}^{(2)}\Gamma^{\mu u}\psi^{(1)} + h.c)$

The solvable solution can be obtained by choosing

$$B_{\mu u}(u) = \frac{B_{\mu u}^{(-1)}}{u} + \underbrace{B_{\mu u}^{(1)}}_{0} u; \qquad m_{B_{\mu u}}^2 = 1,$$

where $B_{\mu u}^{(-1)}$ is a tensor in AdS bulk with a single nonzero component. However, from the boundary point of view, its physical role can be classified as a vector.

SS case. The bulk Dirac equations are given by

$$\partial_u \xi_S^{(SS)} + i[\sigma_0 \otimes \gamma^{\underline{\mu}} k_\mu + \sigma_1 \otimes \gamma^{\underline{\mu}} B_{\mu u}^{(-1)}]\xi_C^{(SS)} = 0, \tag{3.49}$$

$$\partial_u \xi_C^{(SS)} - i[\sigma_0 \otimes \gamma^{\underline{\mu}*} k_\mu - \sigma_1 \otimes \gamma^{\underline{\mu}*} B_{\mu u}^{(-1)}]\xi_S^{(SS)} = 0, \tag{3.50}$$

The main procedure of this type is the same with other interactions. We get the condensation in terms of the source as follows,

$$\mathbb{C}(k) = i[\sigma_0 \otimes \gamma^{\underline{\mu}} k_\mu + \sigma_1 \otimes \gamma^{\underline{\mu}} B_{\mu u}^{(-1)}]^{-1} \mathcal{T}(k)\mathbb{S}(k), \tag{3.51}$$

This yields following Green's function,

$$\mathbb{G}(k_\mu) = -i(\sigma_0 \otimes \sigma_2)[\sigma_0 \otimes \gamma^\mu k_\mu + \sigma_1 \otimes \gamma^\mu B_{\mu u}^{(-1)}]^{-1} \mathcal{T}(k). \tag{3.52}$$

$\boldsymbol{B_{tu}}$/**SS.** By the same calculation in the previous cases, the Green's function is given by

$$\mathbb{G}(k)_{B_{tu}^{(-1)}}^{(SS)} = \frac{1}{2\boldsymbol{k}\mathcal{K}_{tu+}^2 \mathcal{K}_{tu-}^2} \begin{pmatrix} g_{11} & g_{12} \\ g_{21} & g_{22} \end{pmatrix}, \tag{3.53}$$

with $\quad g_{11} = g_{22} = \Big(b(\boldsymbol{k}^2 + \omega^2 - b^2)(\mathcal{K}_- - \mathcal{K}_{tu+}) + |\boldsymbol{k}|(\mathcal{E} - b^2)(\mathcal{K}_{tu-} + \mathcal{K}_{tu+})\Big)\mathbb{K}$

$$+ b\omega\Big(2b|\boldsymbol{k}|(\mathcal{K}_{tu-} + \mathcal{K}_{tu+}) + (\mathcal{E} + b^2)(\mathcal{K}_{tu-} - \mathcal{K}_{tu+})\Big)\sigma_0,$$

$$g_{12} = g_{21} = -\omega\Big(2b|\boldsymbol{k}|(\mathcal{K}_{tu-} + \mathcal{K}_{tu+}) + (\mathcal{E} + b^2)(\mathcal{K}_{tu-} - \mathcal{K}_{tu+})\Big)\mathbb{K} \tag{3.54}$$

$$+ \Big((b^2(\boldsymbol{k}^2 + \omega^2) - \mathcal{E}^2)(\mathcal{K}_{tu-} - \mathcal{K}_{tu+}) - b|\boldsymbol{k}|(\mathcal{E} - b^2)(\mathcal{K}_{tu-} + \mathcal{K}_{tu+})\Big)\sigma_0.$$

where

$$\mathcal{K}_{tu\pm} = \sqrt{(b \pm |\boldsymbol{k}|)^2 - \omega^2}, \quad \mathcal{E} = \boldsymbol{k}^2 - \omega^2, \quad \text{and} \quad b = B_{tu}^{(-1)}. \tag{3.55}$$

The trace of the Green's function turns into a simple form which will be discussed in the following section.

SA case. The bulk Dirac equations are given by

$$(\partial_u - i\Gamma^{\underline{\mu}}B_{\mu u}^{(-1)})\xi_S^{(SA)} - (\sigma_2 \otimes \sigma_0)\Gamma^{\underline{\mu}*}k_\mu\xi_C^{SA} = 0, \tag{3.56}$$

$$(\partial_u - i\Gamma^{\underline{\mu}*}B_{\mu u}^{(-1)})\xi_C^{(SA)} + (\sigma_2 \otimes \sigma_0)\Gamma^{\underline{\mu}}k_\mu\xi_S^{SA} = 0. \tag{3.57}$$

The condensation are given as follows,

$$\mathbb{C}(k) = \frac{\Gamma^{\underline{\mu}*}k_\mu}{\boldsymbol{k}^2 - \omega^2}(\sigma_2 \otimes \sigma_0)[\mathcal{T}(k) - i\Gamma^{\underline{\mu}}B_{\mu u}^{(-1)}]\mathbb{S}(k), \tag{3.58}$$

which yields following retarded Green's function matrix,

$$\mathbb{G}(k)_R = -\frac{\Gamma^{\underline{t}}}{\boldsymbol{k}^2 - \omega^2}\Gamma^{\underline{\mu}}k_\mu[\mathcal{T}(k) - i\Gamma^{\underline{\mu}}B_{\mu u}^{(-1)}]. \tag{3.59}$$

B_{tu}/SA. By the same calculation we have done, the Green's function is given by

$$\mathbb{G}(k)_{B_{tu}^{(-1)}}^{(SS)} = -\frac{1}{2b\omega\boldsymbol{k}}\begin{pmatrix} g_{11} & g_{12} \\ g_{21} & g_{22} \end{pmatrix}, \tag{3.60}$$

with $\quad g_{11} = g_{22}^* = \omega(\mathcal{K}_{tu-} - \mathcal{K}_{tu+})\mathbb{K} + \left(\mathcal{E}(\mathcal{K}_{tu-} - \mathcal{K}_{tu+}) + b\boldsymbol{k}(\mathcal{K}_{tu-} + \mathcal{K}_{tu+})\right)\sigma_0,$

$$g_{12} = g_{21} = \boldsymbol{k}(b^2 + \mathcal{K}_{tu-}\mathcal{K}_{tu+} - \mathcal{E})\sigma_2 \tag{3.61}$$

where $\mathcal{K}_{tu\pm}, \mathcal{E}$ and b are defined in (3.55). We will discuss the trace of the Green's function in the coming section.

B_{xu}/SA/SS. The decomposition and simplification of the Green's functions for this case pose significant challenges. Consequently, we will focus only on the trace of the Green's function, which included in the following section.

3.5 Antisymmetric 2-tensors: $\mathcal{L}_{\text{int}} = B_{\mu\nu}(\bar{\psi}^{(2)}\Gamma^{\mu\nu}\psi^{(1)} + h.c)$

The solvable solution can be obtained by choosing

$$B_{\mu\nu}(u) = \frac{B_{\mu\nu}^{(-1)}}{u} + \underbrace{B_{\mu\nu}^{(1)}}_{0} u; \qquad m_{B_{\mu\nu}}^2 = 1,$$

where $B_{\mu\nu}^{(-1)}$ is symmetry breaking strength constant.

SS case. The bulk Dirac equations are given by

$$[\partial_u - (i\sigma_1 \otimes \gamma^{\underline{\mu\nu}}B_{\mu\nu}^{(-1)})]\xi_S^{(SS)} + i(\sigma_0 \otimes \gamma^{\underline{\mu}}k_\mu)\xi_C^{(SS)} = 0, \tag{3.62}$$

$$[\partial_u + (i\sigma_1 \otimes \gamma^{\underline{\mu\nu}*}B_{\mu\nu}^{(-1)})]\xi_C^{(SS)} - i(\sigma_0 \otimes \gamma^{\underline{\mu}*}k_\mu)\xi_S^{(SS)} = 0, \tag{3.63}$$

Following a similar approach to B_μ's SA-case, we can decouple above equation and get a system of decoupled linear equations. So, we then plugin the solution into the above equation to get

$$\mathbb{C}(k) = i\frac{\sigma_0 \otimes \gamma^{\underline{\mu}*}k_\mu}{\boldsymbol{k}^2 - \omega^2}[\mathcal{T}(k) - (i\sigma_1 \otimes \gamma^{\underline{\mu\nu}})B_{\mu\nu}^{(-1)}]\mathbb{S}(k), \tag{3.64}$$

leads to the Green's function which is given by

$$\mathbb{G}(k)_R = -\frac{\Gamma^{\underline{t}}}{\boldsymbol{k}^2 - \omega^2}(\sigma_1 \otimes \gamma^{\mu*}k_\mu)[\mathcal{T}(k) - (i\sigma_1 \otimes \gamma^{\underline{\mu\nu}})B_{\mu\nu}^{(-1)}]. \tag{3.65}$$

$\boldsymbol{B_{xy}}$/**SS.** By solving the Dirac equations, and plugging-in into (3.65), we get

$$\mathbb{G}(k)_{B_{xy}^{(-1)}}^{(SS)} = \frac{1}{2b_{xy}(k_z^2 - \omega^2)}\begin{pmatrix} g_{11} & g_{12} \\ g_{21} & g_{22} \end{pmatrix}, \tag{3.66}$$

$$\text{with} \quad g_{11} = g_{22} = \Big(|\boldsymbol{k}|(\mathcal{K}_{xy-} - \mathcal{K}_{xy+}) + b(\mathcal{K}_{xy-} + \mathcal{K}_{xy+})\Big)(k_z\sigma_2 - \omega\sigma_0)$$

$$+ \frac{k_z^2 - \omega^2}{|\boldsymbol{k}_\perp|}(\mathcal{K}_{xy-} - \mathcal{K}_{xy+})(k_x\sigma_3 - k_y\sigma_1),$$

$$g_{12} = g_{21} = (k_x\sigma_3 - k_y\sigma_1)(b_{xy}^2 + \mathcal{K}_{xy-}\mathcal{K}_{xy+} - \mathcal{E}). \tag{3.67}$$

where

$$\boldsymbol{k}_\perp^2 = k_x^2 + k_y^2, \quad \mathcal{K}_{xy\pm} = \sqrt{(b_{xy} \pm |\boldsymbol{k}_\perp|)^2 + k_z^2 - \omega^2}, \quad b_{xy} = B_{xy}^{(-1)}, \text{and} \quad \mathcal{E} = \boldsymbol{k}^2 - \omega^2 \tag{3.68}$$

In this case, the singularity $(k_z^2 - \omega^2)^{-1}$ is not changed or canceled by the trace, so that the trace of the Green's function has pole type singularity. We will back to discuss the trace of these Green's functions in the next sections.

SA case. The bulk Dirac equations are given by

$$\partial_u \xi_S^{(SA)} - (\sigma_2 \otimes \sigma_0)[\Gamma^{\underline{\mu}*}k_\mu - \Gamma^{\underline{\mu\nu}}B_{\mu\nu}^{(-1)}]\xi_C^{(SA)} = 0, \tag{3.69}$$

$$\partial_u \xi_C^{(SA)} + (\sigma_2 \otimes \sigma_0)[\Gamma^{\underline{\mu}}k_\mu - \Gamma^{\underline{\mu\nu}*}B_{\mu\nu}^{(-1)}]\xi_S^{(SA)} = 0. \tag{3.70}$$

The above coupled equations can be decoupled to get exact solution of exponential form.

$$\mathbb{C}(k) = [\Gamma^{\underline{\mu}*}k_\mu - \Gamma^{\underline{\mu\nu}}B_{\mu\nu}^{(-1)}]^{-1}(\sigma_2 \otimes \sigma_0)\mathcal{T}(k)\mathbb{S}(k). \tag{3.71}$$

The Green's function for this case is given by

$$\mathbb{G}(k)_R = -(\sigma_3 \otimes \sigma_2)[\Gamma^{\underline{\mu}*}k_\mu - \Gamma^{\underline{\mu\nu}}B_{\mu\nu}^{(-1)}]^{-1}(\sigma_2 \otimes \sigma_0)\mathcal{T}(k). \tag{3.72}$$

$\boldsymbol{B_{xy}}$/**SA.** By the same calculation, the Green's function is given by

$$\mathbb{G}(k)_{B_{xy}^{(-1)}}^{(SA)} = \frac{1}{2\mathcal{K}_{xy+}\mathcal{K}_{xy-}}\begin{pmatrix} g_{11} & g_{12} \\ g_{21} & g_{22} \end{pmatrix}, \tag{3.73}$$

$$\text{with} \quad g_{11} = g_{22}^* = (\mathcal{K}_{xy-} + \mathcal{K}_{xy+})(\mathbb{K}^T - \frac{b_{xy}k_y}{|\boldsymbol{k}_\perp|}\sigma_1) + \frac{b_{xy}k_x}{|\boldsymbol{k}_\perp|}(\mathcal{K}_{xy-} - \mathcal{K}_{xy+})\sigma_3, \tag{3.74}$$

$$g_{12} = g_{21}^* = -\frac{1}{2|\boldsymbol{k}_\perp|}(\mathcal{K}_{xy-} - \mathcal{K}_{xy+})\tilde{\mathbb{K}} - b_{xy}(\mathcal{K}_{xy-} - \mathcal{K}_{xy+})\sigma_0. \tag{3.75}$$

where $\boldsymbol{k}_\perp^2 = k_x^2 + k_y^2$, $\mathcal{K}_{xy\pm}, b_{xy}$ are define in (3.68) and
$\tilde{\mathbb{K}} = \mathbb{K}U\mathbb{K}$, $U = \frac{2}{\boldsymbol{k}^2 - \omega^2}\begin{pmatrix} k_x(k_x - \omega) + k_y(k_y + ik_z) & ik_xk_z + k_y\omega \\ ik_xk_z + k_y\omega & k_x(k_x + \omega) + k_y(k_y - ik_z). \end{pmatrix}$.

$\boldsymbol{B_{tz}}$/**SS/SA.** The decomposition and simplification of the Green's functions for this case pose significant challenges. Consequently, we will focus only on the trace of the Green's function, which included in the following section.
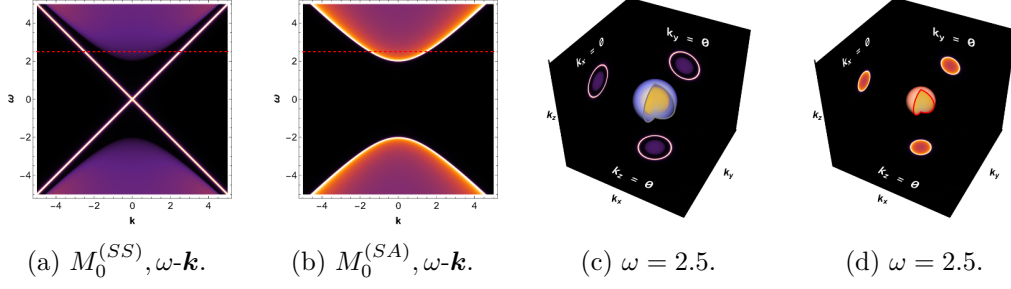
(a) $M_0^{(SS)}, \omega$-$\boldsymbol{k}$. (b) $M_0^{(SA)}, \omega$-$\boldsymbol{k}$. (c) $\omega = 2.5$. (d) $\omega = 2.5$.

Figure 2. Spectral Functions (SFs) of scalar source for both quantization choices. (a,b) SFs in ω-$\boldsymbol{k}$ plane. (c,d) SFs in $\omega = 2.5$ slice, the dashed red line in figure (a), is the three dimensional object in (c,d). The figure at each plane is its projection to each plane. The blue (c) and red (d) surfaces represent the pole and the branch-cut type singularity, respectively.

4 Features of spectral functions

The spectral functions (SF) can be determined by the imaginary part of the traced Green's functions:

$$A(\omega, k) = \text{Im}[\text{Tr}\,(\mathbb{G})]. \tag{4.1}$$

Since the analytic results can be obtained when the order parameter fields have only leading terms we will analyze only such cases.

4.1 Scalar

SS. The essential part of the Green's functions is given by the trace (3.12),

$$\text{Tr}\,\mathbb{G}_{M_0}^{(SS)} = 4\omega \frac{\sqrt{\boldsymbol{k}^2 - \omega^2 + M_0^2}}{\boldsymbol{k}^2 - \omega^2 - i\epsilon}. \tag{4.2}$$

where $\boldsymbol{k}^2 = \sum_{i=1}^{d-1} k_i^2$, and M_0 is the scalar source. The simple pole is located at the surface of the d dimensional cone where d is dimension of the AdS boundary. Notice that the symmetry breaking strength M_0 does not affect the pole structure but only contributes to the gap size. In AdS$_4$, the pair of the gapped spectrum with M_0, M_{50} was reported [24]. In AdS$_5$, we do not have the chiral dynamics of the boundary although we should have corresponding spectrum from the boundary point of view. The difficulty lies in the fact that the chirality cannot be defined in odd dimensions. We postpone this problem to the future work.

SA. The analytic expression is given by

$$\text{Tr}\,\mathbb{G}_{M_0}^{(SA)} = \frac{4\omega}{\sqrt{\boldsymbol{k}^2 - \omega^2 + M_0^2}}, \tag{4.3}$$

The main feature of this interaction is the gap generation, as it was noticed in [24, 38, 39]. Therefore, the scalar source in this case can be interpreted as the mass of boundary fermions. In AdS$_5$, only scalar SA quantization can generate the gap, while in AdS$_4$ case, both M_0, M_{05}^2 can do that. See figure 2(b,d).

Diagonal interaction in fermion flavors. For the scalar, we consider the case where the fermion-scalar interaction is diagonal type, namely,

$$S_{\text{int}} = \int d^5 x \sqrt{-g} \left(\bar{\psi}^{(i)} \Phi \cdot \Gamma \psi^{(i)} + h.c \right).$$

In this case, we have independent sum of two flavors and the result is following.

$$\text{Tr}\, \mathbb{G}_{M_0} = \frac{2\omega}{-M_0 + \sqrt{\boldsymbol{k}^2 - \omega^2 - i\epsilon + M_0^2}} \tag{4.4}$$

Notice that the sign of M_0 is important: for $\text{sign}(M_0) > 0$ we have gapless spectrum while for negative case we have gapped one. Therefore, in the intra-flavor case with $\mathcal{L}_{\text{int}} = i\Phi(\bar{\psi}^{(1)}\psi^{(1)})$, the massless-gapped phase transition depends on the changing sign of M_0 [29]. However, in our inter-flavor with $\mathcal{L}_{\text{int}} = i\Phi(\bar{\psi}^{(2)}\psi^{(1)} + h.c)$, there is no phase transition under the sign change of M_0. See figure 2(a,c). It turns out that for all interaction types other than the scalar-fermion, there is no such phase transition between the gap-gapless phases in the spectral function.

4.1.1 Radial scalar B_u

SS and SA. For this interaction, there is no effect from the order parameter b due to the cancelation that happened during calculation of the Green's function, see (3.24). In fact, this has been a puzzle from the view of the numerical calculation. As a result, the trace of the Green's function, regardless the quantization choice, is given by

$$\text{Tr}\, \mathbb{G}_{B_u^{(0)}}^{(SS,SA)} = \frac{4\omega}{\sqrt{\boldsymbol{k}^2 - \omega^2}}, \tag{4.5}$$

which is the same as that of critical point where $B_u = 0$.

4.2 Vectors

4.2.1 Time-like polar vector, B_t

SS. The trace of the Green's matrix (3.32), by choosing $\mu = t$ is given by

$$\text{Tr}\, \mathbb{G}_{B_t^{(0)}}^{(SS)} = 2 \left(\frac{b + \omega}{\sqrt{\boldsymbol{k}^2 - (b + \omega)^2}} - \frac{b - \omega}{\sqrt{\boldsymbol{k}^2 - (b - \omega)^2}} \right), \tag{4.6}$$

where $\boldsymbol{k}^2 = \sum_i^{d-1} k_i^2$. In this case, above result shows two Dirac cones, shifted along $\pm\omega$ directions, which are not interacting with each other. The singularities are located at each cone. Notice that there are spherical symmetry in k_x-k_y-k_z. See figure 3(a,b,c)

SA. The trace of the Green's matrix (3.44) is given by

$$\text{Tr}\, \mathbb{G}_{B_t^{(0)}}^{(SA)} = \frac{2}{b} \left[\sqrt{\boldsymbol{k}^2 - (b - \omega)^2} - \sqrt{\boldsymbol{k}^2 - (b + \omega)^2} \right], \tag{4.7}$$

In this case, the symmetry are the same with SS case. However, there is no singularity in the Green's function. Therefore the entire SF is described by a branch-cut without singularity. See figure 3(d,e,f)
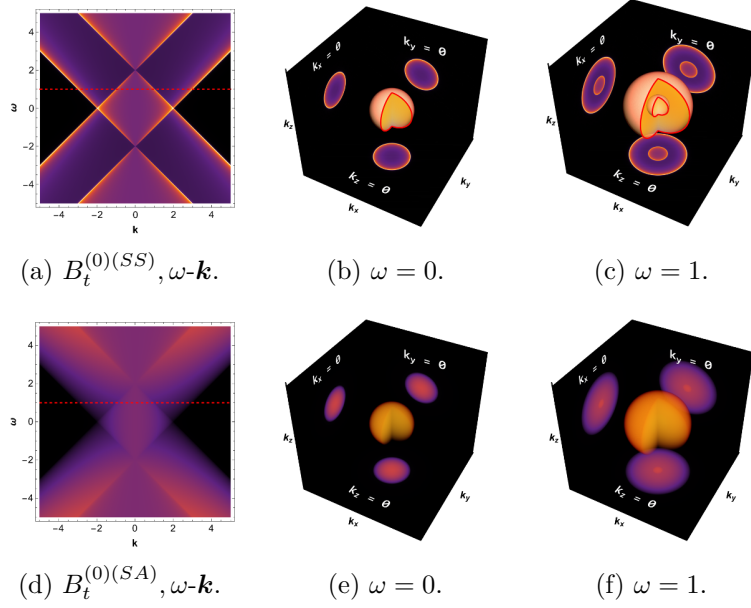
(a) $B_t^{(0)(SS)}, \omega\text{-}\boldsymbol{k}$. (b) $\omega = 0$. (c) $\omega = 1$.

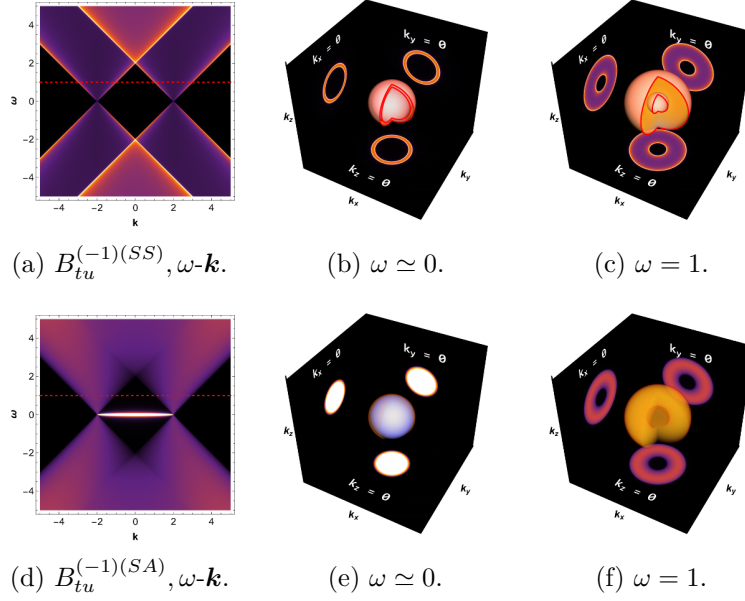(d) $B_t^{(0)(SA)}, \omega\text{-}\boldsymbol{k}$. (e) $\omega = 0$. (f) $\omega = 1$.

Figure 3. Spectral functions (SFs) of B_t source for both quantization choices. (a,d) SFs in $\omega\text{-}\boldsymbol{k}$ plane. (b,e) SFs in $\omega = 0$ plane, and (c,f) for $\omega = 1$ plane corresponding to the dashed red line, in which the background represents the certain slices at each momentum is zero. The bare orange bulk without the surface shows the spectral function without singularity.

4.2.2 Time-like radial vector B_{tu}

SS. The analytic expression is given by

$$\operatorname{Tr}\mathbb{G}^{(SS)}_{B_{tu}^{(-1)}} = \frac{2\omega}{\sqrt{(b - |\boldsymbol{k}|)^2 - \omega^2}} + \frac{2\omega}{\sqrt{(b + |\boldsymbol{k}|)^2 - \omega^2}}. \tag{4.8}$$

In this case, the spectrum is isotropic for each Dirac cone shifted along the entire $\boldsymbol{k}$-space, and that is why we cannot distinguish the spectrum of $B_{xy(SA)}$ and $B_{tu(SA)}$ in AdS_4. However, in AdS_5, the SF has spherical symmetry, while B_{xy} spectrum has planar rotational symmetry in k_x-k_y plane. See figure 4(a,b,c).

SA. The analytic expression is given by

$$\operatorname{Tr}\mathbb{G}^{(SA)}_{B_{tu}^{(-1)}} = -\frac{2}{b}\left[\frac{(b + |\boldsymbol{k}|)\sqrt{(b - |\boldsymbol{k}|)^2 - \omega^2} + (b - |\boldsymbol{k}|)\sqrt{(b + |\boldsymbol{k}|)^2 - \omega^2}}{\omega + i\epsilon}\right]. \tag{4.9}$$

The pole-type singularity appears in this case as a flat band. In AdS$_5$, It is a 3D flat band in the solid sphere with radius b. See figure 4(d,e). However, the flat band immediately disappears if move to $\omega \neq 0$ slice. See figure 4(f).

4.2.3 Space-like polar vector, B_x

SS. The trace of the Green's matrix (3.32), by choosing $\mu = x$

$$\operatorname{Tr}\mathbb{G}^{(SS)}_{B_x^{(0)}} = \frac{2\omega}{\sqrt{(b - k_x)^2 + \boldsymbol{k}_\perp^2 - \omega^2}} + \frac{2\omega}{\sqrt{(b + k_x)^2 + \boldsymbol{k}_\perp^2 - \omega^2}}, \tag{4.10}$$

Figure 4. Spectral functions (SFs) for B_{tu} source for both quantization choices. (a,c) SFs in ω-$\boldsymbol{k}$ plane. (b,c),(e,f) SFs in k_x-k_y-k_z at $\omega = 0, 1$ slices, respectively.

(a) $B_{tu}^{(-1)(SS)}, \omega$-$\boldsymbol{k}$. (b) $\omega \simeq 0$. (c) $\omega = 1$.

(d) $B_{tu}^{(-1)(SA)}, \omega$-$\boldsymbol{k}$. (e) $\omega \simeq 0$. (f) $\omega = 1$.

where $\boldsymbol{k}_\perp^2 = k_y^2 + k_z^2$. The SF shows the superposition of two Dirac cones shifted along the k_x direction, which are non-interacting with each other. (4.10). The distance between the Dirac points is $2b$ and the surface of the cones are branch-cut type singularity. Notably, the SF in the ω-k_x plane exhibits a shifting of 2dimensional Dirac cones, see fig 5(a). In the section of ω-$k_\perp$ plane; it shows a gap, see figure 5(b).

SA. The trace of the Green's function matrix (3.44) for $\mu = x$ is given by

$$\operatorname{Tr} \mathbb{G}_{B_x^{(0)}}^{(SA)} = \frac{2\omega}{b} \left[\frac{(b + k_x)\sqrt{(b - k_x)^2 + \boldsymbol{k}_\perp^2 - \omega^2} + (b - k_x)\sqrt{(b + k_x)^2 + \boldsymbol{k}_\perp^2 - \omega^2}}{\boldsymbol{k}_\perp^2 - \omega^2 - i\epsilon} \right]. \quad (4.11)$$

The main feature of the spectrum is shifted Dirac cones in $\pm k_x$ direction: two Dirac points is connected by flat band of 1-dimensional pole singularity $(\omega^2 - \boldsymbol{k}_\perp^2)^{-1}$ along $k_x \in [-b, b]$. See figure 5(e,f). It is important to note that the residue is zero for $k_x \notin [-b, b]$, so there is no singularity outside the interval. See figure 5(g,h).

4.2.4 Space-like radial vector, B_{ux}

The analytic expression is given by

$$\operatorname{Tr} \mathbb{G}_{B_{ux}^{(-1)}}^{(SS)} = 4\omega \frac{b^2 + \boldsymbol{k}^2 - \omega^2 + f_+ f_-}{f_+ f_- (f_+ + f_-)}, \quad (4.12)$$

$$\operatorname{Tr} \mathbb{G}_{B_{ux}^{(-1)}}^{(SA)} = 4\omega \frac{(f_+ + f_-)\sqrt{\omega^2 - \boldsymbol{k}_\perp^2} - b(f_+ - f_-)}{\sqrt{\omega^2 - \boldsymbol{k}_\perp^2}(b^2 + \boldsymbol{k}^2 - \omega^2 + f_+ f_-)}. \quad (4.13)$$
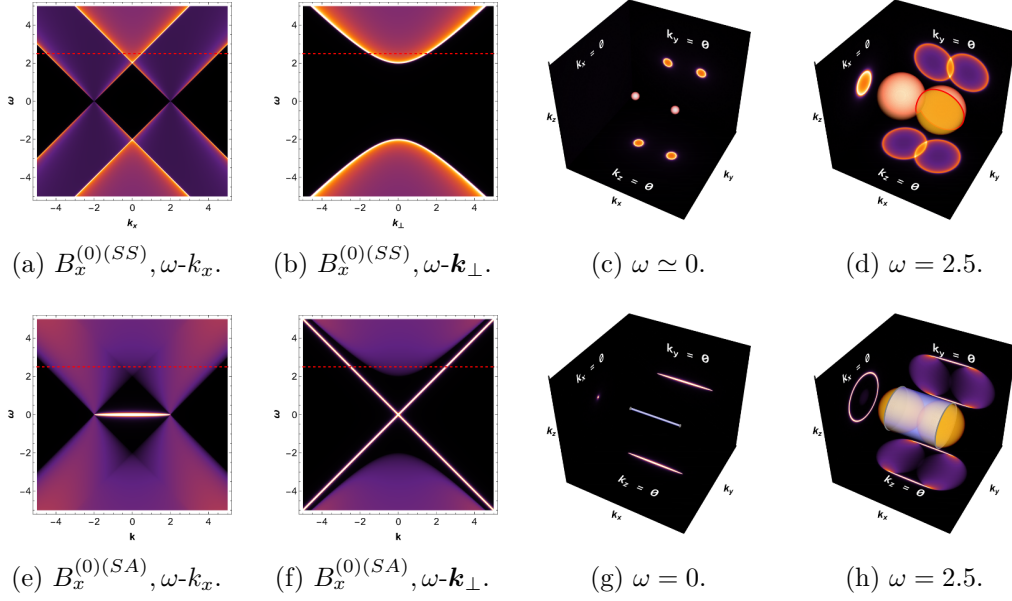
Figure 5. Spectral functions (SFs) of B_x source for both quantization choices. (a,b,e,f) SFs in ω-k_x, ω-$\boldsymbol{k}_\perp$ plane. (c,g) SFs in $\omega = 0$, and (d,h) SFs for $\omega = 2.5$ correspondingly to the dashed red lines. In (g,h), if $k_x \notin [-b, b]$ the pole type singularity disappears so that only $k_x \notin [-b, b]$ which the arc lines visible. The box's background represents the certain slices at each momentum is zero.

where $f_\pm = \sqrt{k_x^2 - \left(b \pm \sqrt{\omega^2 - \boldsymbol{k}_\perp^2}\right)^2}$. The structure of the $f_\pm$ is nothing but shifting of $|\omega|$-radius semispheres in k_x direction. It is useful to realize that $f_- f_+$ is shifting of two $|\omega|$-radius spheres in k_x direction. See figure 6.

4.3 Antisymmetric 2-tensors

4.3.1 Space-like tensor B_{xy}

SS. The polar spatial tensor source of SS-quantization yields Green's functions with the rotational symmetry in k_x-k_y plane. The trace of the Green's function matrix (3.65) yields

$$\mathrm{Tr}\, \mathbb{G}^{(SS)}_{B_{xy}^{(-1)}} = \frac{2\omega}{b} \left[\frac{(b + |\boldsymbol{k}_\perp|)\sqrt{(b - |\boldsymbol{k}_\perp|)^2 + k_z^2 - \omega^2} + (b - |\boldsymbol{k}_\perp|)\sqrt{(b + |\boldsymbol{k}_\perp|)^2 + k_z^2 - \omega^2}}{k_z^2 - \omega^2 - i\epsilon} \right]. \tag{4.14}$$

Where $\boldsymbol{k}_\perp^2 = k_x^2 + k_y^2$, which is perpendicular to k_z. The structure of SF is different to B_x case due to rotational symmetry in k-space. In this case, the cone shifts along $\boldsymbol{k}_\perp$ directions, which makes the nodal line instead of separated two-Dirac points. Meanwhile, an infinite 1-dimensional pole-type singularity exists on a disk $\boldsymbol{k}_\perp \in [-b, b]$. See figure 7(e,f) In k_x-k_y-k_z space, if ω slightly increases from 0, the singularity splits in k_z direction and connects the torus's center; see figure 7(g,h). For AdS4, we lost the third momentum, so that no cone appears and flat band remains only in k_x-k_y plane [40].

SA. The spectrum exhibits a notable characteristic of rotational symmetry in the k_x-k_y plane (4.15), so the nodal line is this case's main feature. The radius of the nodal line is 2b,
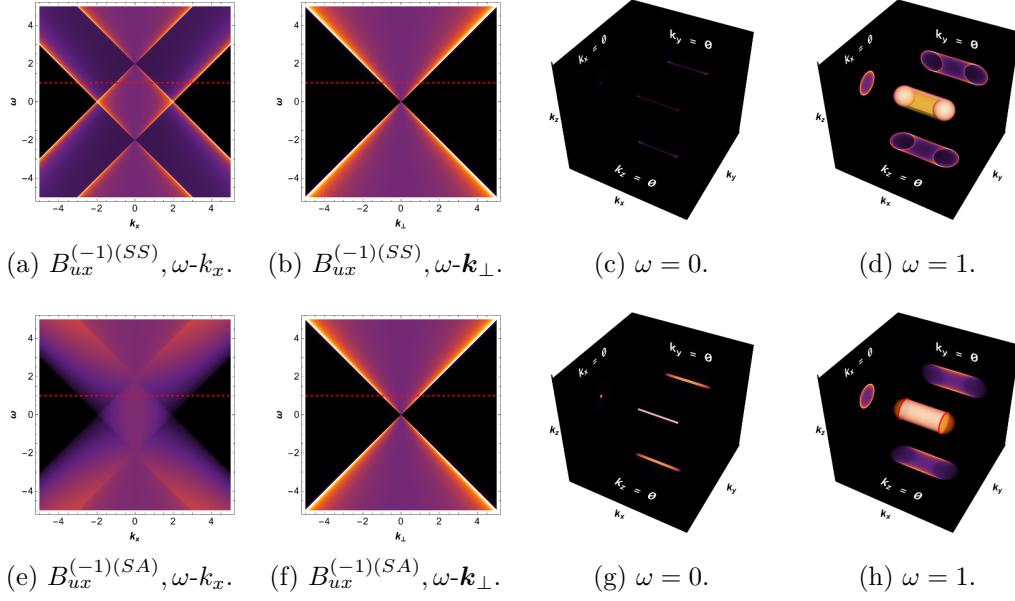
(a) $B_{ux}^{(-1)(SS)}, \omega\text{-}k_x.$ (b) $B_{ux}^{(-1)(SS)}, \omega\text{-}\boldsymbol{k}_\perp.$ (c) $\omega = 0.$ (d) $\omega = 1.$

(e) $B_{ux}^{(-1)(SA)}, \omega\text{-}k_x.$ (f) $B_{ux}^{(-1)(SA)}, \omega\text{-}\boldsymbol{k}_\perp.$ (g) $\omega = 0.$ (h) $\omega = 1.$

Figure 6. Spectral functions (SFs) for B_{ux} source for both quantization choices. (a,b,e,f) SFs in $\omega\text{-}\boldsymbol{k}$ plane. (c,d,g,h) SFs in $k_x\text{-}k_y\text{-}k_z$ at $\omega = 0, 1$ slices, respectively. The spectral features are analogous to B_x case, with extra branch-cut singularity pieces. Notice that the spectrum shown in (g) is just the nonsingular branch-cut.

and the surface of the SF appears as the branch-cut type singularity. See figure 7(a,b,c,d)

$$\mathrm{Tr}\,\mathbb{G}_{B_{xy}^{(-1)}}^{(SA)} = \frac{2\omega}{\sqrt{(b - |\boldsymbol{k}_\perp|)^2 + k_z^2 - \omega^2}} + \frac{2\omega}{\sqrt{(b + |\boldsymbol{k}_\perp|)^2 + k_z^2 - \omega^2}}. \tag{4.15}$$

4.3.2 Time-space-like tensor B_{tz}

The trace of the Green's function is given by

$$\mathrm{Tr}\,\mathbb{G}_{B_{tz}^{(-1)}}^{(SA)} = 4\omega\frac{b^2 + \boldsymbol{k}^2 - \omega^2 + h_+ h_-}{h_+ h_- (h_+ + h_-)}, \tag{4.16}$$

$$\mathrm{Tr}\,\mathbb{G}_{B_{tz}^{(-1)}}^{(SS)} = 4\omega\frac{(h_+ + h_-)\sqrt{\omega^2 - \boldsymbol{k}_\perp^2} - b(h_+ - h_-)}{\sqrt{\omega^2 - \boldsymbol{k}_\perp^2}(b^2 + \boldsymbol{k}^2 - \omega^2 + h_+ h_-)}. \tag{4.17}$$

where $h_\pm = \sqrt{\boldsymbol{k}_\perp^2 - \left(b \pm \sqrt{\omega^2 - k_z^2}\right)^2}$, $h_\pm$ has a semi-torus structure. Here, $h_- h_+ = \sqrt{\left((b - |\boldsymbol{k}_\perp|)^2 + k_z^2 - \omega^2\right)\left((b + |\boldsymbol{k}_\perp|)^2 + k_z^2 - \omega^2\right)}$, which is nothing other than a torus. This structure analogous to B_{xy} with extra branch-cut singularity pieces. For SA case at nonzero ω, we observe a torus with connecting planes. See figure 8(d). For SS case at nonzero ω, it is branch-cut version of $B_{xy}^{(SS)}$. See figure 8(h). The crucial difference is that there is no singularity at $\omega = 0$ in SS case.

Until now, we have successfully obtained spectral functions for all interaction and quantization types where the condensate of field $\langle \mathcal{O}_\Phi \rangle = 0$. Our analytic results are summarized in table 1, which allows us to classify them based on their spectral features into the following four classes:
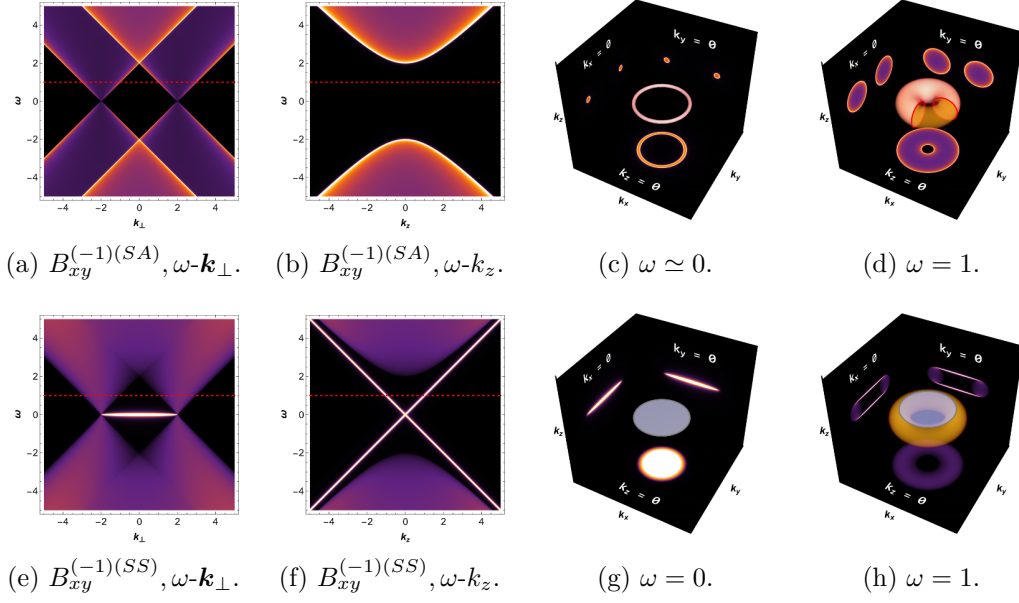
Figure 7. Spectral function (SFs) of B_{xy} source for both quantization choices. (a,b,e,f) SFs in ω-k_x, ω-$\boldsymbol{k}_\perp$ planes. (c,g,) SFs in $\omega = 0$, and (d,h) $\omega = 1$ correspondingly to the dashed red lines. The spectral functions have rotational symmetry for each fixing k_z. The background of the box represents the certain slices at each momentum is zero.
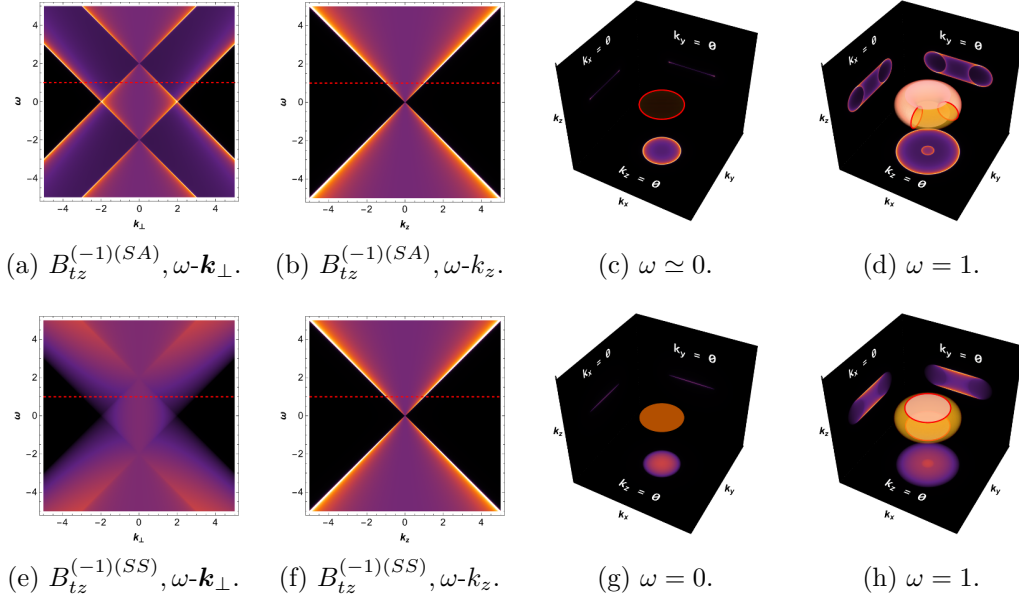

Figure 8. Spectral functions (SFs) for B_{tx} source for both quantization choices. (a,b,e,f) SFs in ω-$\boldsymbol{k}$ plane. (c,d,g,h) SFs in k_x-k_y-k_z at $\omega = 0, 1$ slices, respectively. The spectral features are analogous to B_{xy}. Notice that the disk appearing in (g) is just the nonsingular branch-cut.

i) Flat band and topological liquid. The main characteristic of this class is the simple-pole type singularity. It should be noted that these flat bands appear in a finite region, which differs from flat bands that usually appear in lattice models. An explanation why our flat bands appear over the finite region will be provided in the upcoming subsection. The first column of figure 9 shows this class.

ii) Gaps and shifting of Dirac cones along $\boldsymbol{k}$-direction. This class includes gaps in the s-, p-wave, nodal ring, and nodal shell. The branch-cut type singularity is the only singularity type in this class. The second column of figure 9 depicts this class.

iii) Gapless with nonsingular. Spectral features of this class are analogous to the first class; however, there is no particle excitation at $\omega = 0$ since there is no singularity. Therefore, we will call them nonsingular segments, disks, and bowls. The third column of figure 9 represents this class.

iv) Gapless with shifting in ω-direction. Spectral features of this class show some similarities to the gaps class, but instead of the usual nodal segment, ring, or shell, we found non-zero spectra inside. Therefore, we will call them filled nodal segment, ring, or shell, distinguishing them from the second class. The fourth column of figure 9 illustrates this class.

4.4 Emergence of various dimensions flat band over finite region

We have shown that various dimensions flat band can emerge in our holographic approach after the symmetry is broken by Φ, B_i, B_{ij}, and B_{tu}. We have reported the existance of these flat bands in our previous works by numerical study. Nevertheless, the reason the flat band emerged just over the finite region was still being investigated.

According to our analytic results, the problem is clarified. Firstly, the flat band's singularity can be confirmed as a simple pole by directly calculating residue for each case. Secondly, we found that where the frequency approaches the momentum which makes the Green's function diverge, then the imaginary of the $\mathrm{Tr}\,\mathbb{G}$ can be approximately written in terms of the step-function as follows:

- Scalar M_0:
$$\mathrm{Im}[\mathrm{Tr}\,\mathbb{G}_{M_0}^{(SS)}]\Big|_{\omega^2 \to \boldsymbol{k}^2} \simeq \mathrm{Im}\left[\frac{4\omega|M_0|}{\boldsymbol{k}^2 - \omega^2 - i\epsilon}\right], \tag{4.18}$$

- Space-like polar vector B_x:
$$\mathrm{Im}[\mathrm{Tr}\,\mathbb{G}_{B_x^{(0)}}^{(SA)}]\Big|_{\omega^2 \to \boldsymbol{k}_\perp^2} \simeq \mathrm{Im}\left[\frac{2\omega(b_x^2 - k_x^2)}{\boldsymbol{k}_\perp^2 - \omega^2 - i\epsilon}\right]\Theta(b_x^2 - k_x^2), \tag{4.19}$$

- Space-like polar tensor B_{xy}:
$$Im[\mathrm{Tr}\,\mathbb{G}_{B_{xy}^{(-1)}}^{(SS)}]\Big|_{\omega^2 \to k_z^2} \simeq \mathrm{Im}\left[\frac{2\omega(b^2 - \boldsymbol{k}_\perp^2)}{k_z^2 - \omega^2 - i\epsilon}\right]\Theta(b^2 - \boldsymbol{k}_\perp^2), \tag{4.20}$$

- Time-like radial vector B_{tu}:
$$\mathrm{Im}[\mathrm{Tr}\,\mathbb{G}_{B_{tu}^{(-1)}}^{(SA)}]\Big|_{\omega \to 0} \simeq -\mathrm{Im}\left[\frac{2(b^2 - \boldsymbol{k}^2)}{\omega - i\epsilon}\right]\Theta(b^2 - \boldsymbol{k}^2). \tag{4.21}$$

Interactions	Trace of analytic Green's functions (AdS$_5$)		Features/Classifications	Singularity types
M_0	$\operatorname{Tr}\mathbb{G}^{(SA)}_{M_0} = \dfrac{4\omega}{\sqrt{\boldsymbol{k}^2 - \omega^2 + M_0^2}}$	(4.3)	Gapful/s-wave gap	Branch-cut
	$\operatorname{Tr}\mathbb{G}^{(SS)}_{M_0} = 4\omega\dfrac{\sqrt{\boldsymbol{k}^2 - \omega^2 + M_0^2}}{\boldsymbol{k}^2 - \omega^2 - i\epsilon}$	(4.2)	Topological liquid	Pole
B_x	$\operatorname{Tr}\mathbb{G}^{(SS)}_{B_x^{(0)}} = \dfrac{2\omega}{\sqrt{(b-k_x)^2 + \boldsymbol{k}_\perp^2 - \omega^2}} + \dfrac{2\omega}{\sqrt{(b+k_x)^2 + \boldsymbol{k}_\perp^2 - \omega^2}}$	(4.10)	Shifting cones/p-wave gap	Branch-cut
	$\operatorname{Tr}\mathbb{G}^{(SA)}_{B_x^{(0)}} = \dfrac{2\omega}{b}\left[\dfrac{(b+k_x)\sqrt{(b-k_x)^2 + \boldsymbol{k}_\perp^2 - \omega^2} + (b-k_x)\sqrt{(b+k_x)^2 + \boldsymbol{k}_\perp^2 - \omega^2}}{\boldsymbol{k}_\perp^2 - \omega^2 - i\epsilon}\right]$	(4.11)	1D flat band	Pole
B_{xy}	$\operatorname{Tr} G^{(SA)}_{B_{xy}^{(-1)}} = \dfrac{2\omega}{\sqrt{(b-|\boldsymbol{k}_\perp|)^2 + k_z^2 - \omega^2}} + \dfrac{2\omega}{\sqrt{(b+|\boldsymbol{k}_\perp|)^2 + k_z^2 - \omega^2}}$	(4.15)	Nodal ring	Branch-cut
	$\operatorname{Tr}\mathbb{G}^{(SS)}_{B_{xy}^{(-1)}} = \dfrac{2\omega}{b}\left[\dfrac{(b+|\boldsymbol{k}_\perp|)\sqrt{(b-|\boldsymbol{k}_\perp|)^2 + k_z^2 - \omega^2} + (b-|\boldsymbol{k}_\perp|)\sqrt{(b+|\boldsymbol{k}_\perp|)^2 + k_z^2 - \omega^2}}{k_z^2 - \omega^2 - i\epsilon}\right]$	(4.14)	2D flat band	Pole
B_{tu}	$\operatorname{Tr}\mathbb{G}^{(SS)}_{B_{tu}^{(-1)}} = \dfrac{2\omega}{\sqrt{(b-|\boldsymbol{k}|)^2 - \omega^2}} + \dfrac{2\omega}{\sqrt{(b+|\boldsymbol{k}|)^2 - \omega^2}}$	(4.8)	Nodal shell	Branch-cut
	$\operatorname{Tr}\mathbb{G}^{(SA)}_{B_{tu}^{(-1)}} = -\dfrac{2}{b}\left[\dfrac{(b+|\boldsymbol{k}|)\sqrt{(b-|\boldsymbol{k}|)^2 - \omega^2} + (b-|\boldsymbol{k}|)\sqrt{(b+|\boldsymbol{k}|)^2 - \omega^2}}{\omega + i\epsilon}\right]$	(4.9)	3D flat band	Pole
B_u	$\operatorname{Tr}\mathbb{G}^{(SS)}_{B_u^{(0)}} \equiv \operatorname{Tr}\mathbb{G}^{(SA)}_{B_u^{(0)}} = \dfrac{4\omega}{\sqrt{\boldsymbol{k}^2 - \omega^2}}$	(4.5)	QCP	Branch-cut
B_{ux}	$\operatorname{Tr}\mathbb{G}^{(SS)}_{B_{ux}^{(-1)}} = 4\omega\dfrac{b^2 + \boldsymbol{k}^2 - \omega^2 + f_+ f_-}{f_+ f_- (f_+ + f_-)};\ f_\pm = \sqrt{k_x^2 - \left(b \pm \sqrt{\omega^2 - \boldsymbol{k}_\perp^2}\right)^2}$	(4.12)	Filled nodal segment	Branch-cut
	$\operatorname{Tr}\mathbb{G}^{(SA)}_{B_{ux}^{(-1)}} = 4\omega\dfrac{(f_+ + f_-)\sqrt{\omega^2 - \boldsymbol{k}_\perp^2} - b(f_+ - f_-)}{\sqrt{\omega^2 - \boldsymbol{k}_\perp^2}(b^2 + \boldsymbol{k}^2 - \omega^2 + f_+ f_-)};\ f_\pm = \sqrt{k_x^2 - \left(b \pm \sqrt{\omega^2 - \boldsymbol{k}_\perp^2}\right)^2}$	(4.13)	Non-singular segment	Branch-cut & nonsingular
B_{tz}	$\operatorname{Tr}\mathbb{G}^{(SA)}_{B_{tz}^{(-1)}} = 4\omega\dfrac{b^2 + \boldsymbol{k}^2 - \omega^2 + h_+ h_-}{h_+ h_- (h_+ + h_-)};\ h_\pm = \sqrt{\boldsymbol{k}_\perp^2 - \left(b \pm \sqrt{\omega^2 - k_z^2}\right)^2}$	(4.16)	Filled nodal ring	Branch-cut
	$\operatorname{Tr}\mathbb{G}^{(SS)}_{B_{tz}^{(-1)}} = 4\omega\dfrac{(h_+ + h_-)\sqrt{\omega^2 - \boldsymbol{k}_\perp^2} - b(h_+ - h_-)}{\sqrt{\omega^2 - \boldsymbol{k}_\perp^2}(b^2 + \boldsymbol{k}^2 - \omega^2 + h_+ h_-)};\ h_\pm = \sqrt{\boldsymbol{k}_\perp^2 - \left(b \pm \sqrt{\omega^2 - k_z^2}\right)^2}$	(4.17)	Non-singular disk	Branch-cut & nonsingular
B_t	$\operatorname{Tr}\mathbb{G}^{(SS)}_{B_t^{(0)}} = 2\left(\dfrac{b+\omega}{\sqrt{\boldsymbol{k}^2 - (b+\omega)^2}} - \dfrac{b-\omega}{\sqrt{\boldsymbol{k}^2 - (b-\omega)^2}}\right)$	(4.6)	Filled nodal shell	Branch-cut
	$\operatorname{Tr}\mathbb{G}^{(SA)}_{B_t^{(0)}} = \dfrac{2}{b}\left[\sqrt{\boldsymbol{k}^2 - (b-\omega)^2} - \sqrt{\boldsymbol{k}^2 - (b+\omega)^2}\right]$	(4.7)	Non-singular bowl	Branch-cut & nonsingular

Table 1. The summary of trace of Green's functions, spectral features and classifications for AdS$_5$. For all of the expressions, $\boldsymbol{k}^2 = k_x^2 + k_y^2 + k_z^2$.

It is clear that apart from the scalar case, the simple pole spectra are nonzero, just over a finite region, due to the presence of step functions. It also explains why the flat band of $B_{tu}^{(SA)}$ appears just over a finite region even if the singularity is $\boldsymbol{k}$ independent function ($1/\omega$). According to these observations, we classify them as various dimensions flat bands: 1,2, and 3-dimensional flat bands as shown in figure 9.

4.5 Spectrum in the presence of the order parameter's condensation

We have exhibited the SFs corresponding to the condensation in the alternative quantization by employing the analytic Green's functions. Here we mention that the flow equation can numerically compute the case where order parameter fields condensation in the standard quantization [38–40] although the analytic expressions are not possible. The spectral features in the probe limit can be generated by employing seven spectral features and modifying the symmetry in $\boldsymbol{k}$-space.
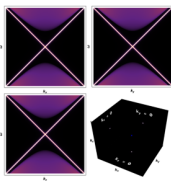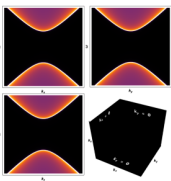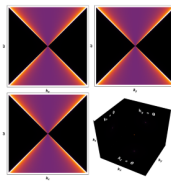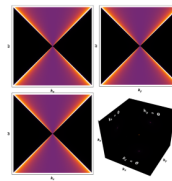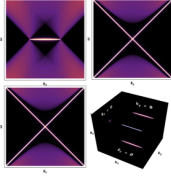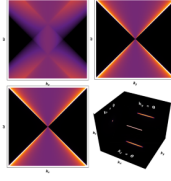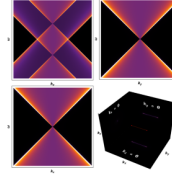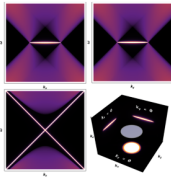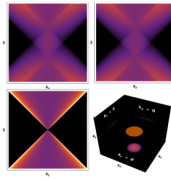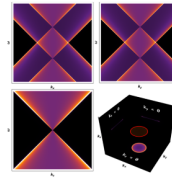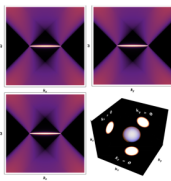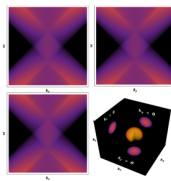
Figure 9. The classifications of spectral features for all interaction and quantization types. The table consists of spectral functions in ω-$k_{x,y,z}$ and k_x-k_y-k_z at $\omega \simeq 0$. The spectra have identical symmetry on the horizontal alignment and have the same spectral feature on the vertical alignment. d_{eff} is the number of the flat band, cones k-shifting, nonsingular, and cones ω-shifting spectra appearing in each **k**-space section.

Our calculation shows that the interactions leading to the simple pole type in the alternative quantization, which are given by $\Phi, B_x, B_{xy}, B_{tu}$, also yield the simple pole types singularity in the standard quantized case as well. But not vice versa. For example, the scalar interaction with standard quantization have poles in SA fermion, but in alternative quantization has branch-cut in the same SA fermion. See figure 10(b). In contrast, the remaining interactions B_u, B_{ux}, B_{tz}, B_t yield branch-cut type Green's functions alternative quantization. See figure 10.

In this section, we found three types of Green's function: pole type, branch-cut type singularity and branch-cut non-singularity. In the upcoming section, we will compute the full back-reaction for each order parameter field. It is noteworthy that we have observed a remarkably stable pole-type singularity. This observation agrees with our previous research,
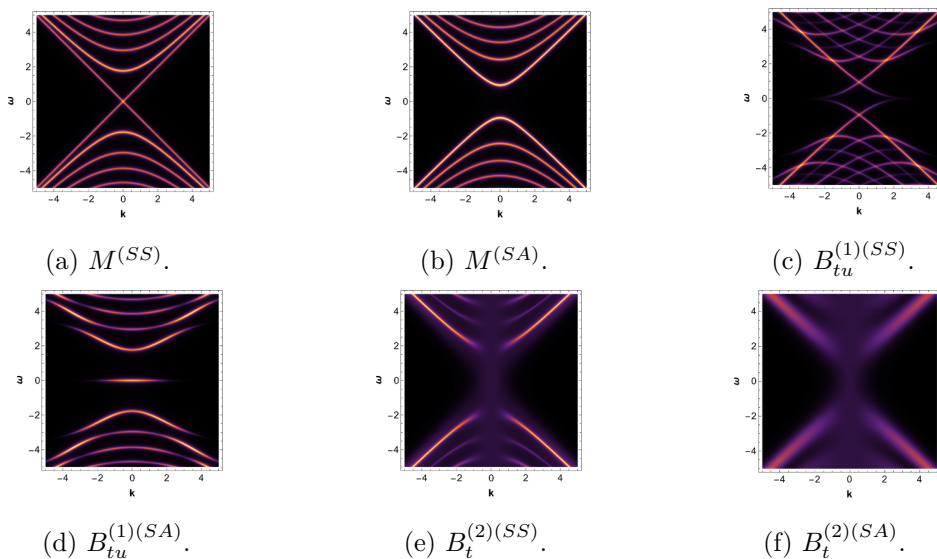
(a) $M^{(SS)}$.

(b) $M^{(SA)}$.

(c) $B_{tu}^{(1)(SS)}$.

(d) $B_{tu}^{(1)(SA)}$.

(e) $B_t^{(2)(SS)}$.

(f) $B_t^{(2)(SA)}$.

Figure 10. Spectral functions (SFs) which are associated with the condensation order parameter fields. (a,b) and (c,d) scalar and B_{tu} condensation SFs, lead to the complete disappearance of the fuzzy spectra, resulting in the emergence of only the Kaluza-Klein (KK) modes. Notice that in the source case of these interactions, both simple pole and branch-cut singularities can occur. However, only the simple pole type is observed in the condensation cases. (e,f) B_t condensation, the types of Green's functions appear similar to those observed in the source cases. Keep in mind that combining these SFs and introducing variations makes it possible to generate all 16 types of interaction SFs.

wherein we interpreted the pole type, referred to as the zero mode, as a topological mode. The stability of this mode is assured by the boundary conditions of the fermions, which makes it topological [29]. Additionally, we also give the Green's functions, dualities, and the classifications for AdS$_4$ theory in A.

5 Backreacted spectral functions

So far, our calculations were done in the probe limit, where back-reactions to the metric by the order parameter fields were neglected. Consequently, the reliability of these approximate analytic expressions can be asked and the only way to answer is to carry out the full back-reacted solution. In this section, we carry out this program and compare it with the essential probe limit analytic results. Since any of the back reaction calculations involve full-scale numerical work, and preliminary calculation with low numerical grid gave us the tentative result that the Green's function with pole type singularity is stable under perturbation while the branch cut type singularity is not. Therefore we also expect that the full-scale back reacktion should be similar. In this section, we perform only for the space-like antisymmetric tensor type order parameter, postponing other cases to future work. We use a special lagrangian, which permits the non-zero source and zero condensation. In other words, we use the theory that allowed the alternative quantization of the order parameter field. We should mention a big difference between the order parameter field B_t, and the usual gauge field A_t, which is not an order parameter but a field encoding the charge density effect provided

externally. The charge density ρ is given by external condition and the horizon regularity fixes its value μ at the boundary so that $A_t \sim \mu - \rho u^2$. Therefore, A_t can not describe any broken symmetry or order parameter. On the other hand, B_t is supposed to describe the spontaneous symmetry breaking by having zero source or zero condensation. It turns out that this is possible only by coupling with other fields. Just as in the superconductivity case, we assumed it is induced mainly by an interaction with the gauge field, $F = dA$. In this section, where we actually produces such field B_t by considering back reaction and coupling, we used $F_{\mu\nu}^2 B_\alpha^2$ for the vector. This comment applies to all other tensor fields as well.

We follow the fundamental action model, which is given in [41, 42]. Additionally, to quantize real B_{xy} alternatively, where only the leading term is nonvanishing, we introduce A_t and set the highest order coupling term between A_t and B_{xy} as the source of spontaneous symmetry breaking. The model is then given by

$$ \mathcal{S}_{g,B,A} = \int d^5x \sqrt{-g} \left(R - 2\Lambda - \frac{1}{4} F_{\mu\nu}^2 \left(1 + 4\gamma B_{\alpha\beta}^2 \right) - \frac{1}{3} H_{\lambda\alpha\beta}^2 - m^2 B_{\alpha\beta}^2 \right), \qquad (5.1) $$

here $A = A_t(u)dt$ and the antisymmetric field-strength tensor $H_{\lambda\alpha\beta}$, given by

$$ H_{\lambda\mu\nu} = \nabla_\lambda B_{\alpha\beta} + \nabla_\alpha B_{\beta\lambda} + \nabla_\beta B_{\lambda\alpha} \,; \qquad \nabla_\lambda B_{\alpha\beta} = \partial_\lambda B_{\alpha\beta} - \Gamma_{\lambda\alpha}^\gamma B_{\gamma\beta} - \Gamma_{\lambda\beta}^\sigma B_{\alpha\sigma}, \qquad (5.2) $$

where $B = B_{xy}(u) \, dx \wedge dy$. Notice that the choice of our $A_\mu, B_{\alpha\beta}$, leading to $F^{\mu\nu} B_{\alpha\beta} = 0$, and in this scenario, $F_{\mu\nu}^2 B_{\alpha\beta}^2$ becomes the highest order term.

It is important to note that by setting $m^2 = 1$, the asymptotic behaviour of space-like antisymmetric 2-tensor field $B_{xy}(u)$ is given by

$$ B_{xy}(u) \simeq \langle \mathcal{O}_1 \rangle u^{-1} + \langle \mathcal{O}_2 \rangle u + \cdots . \qquad (5.3) $$

The presence of the singularity in the expression causes some numerical difficulties; consequently, we define a new variable, $\mathcal{B}_{xy}(u) := uB_{xy}(u)$ which significantly enhances numerical convenience by eliminating the singularity from the expression. With a small value ϵ, we can determine the sub-leading term $\langle \mathcal{O}_2 \rangle$ by $\mathcal{B}_{xy}'(\epsilon)/2\epsilon$, which suppose to be zero due to the alternative quantization.

In the back-reaction calculation, we take the following ansatz,

$$ ds^2 = \frac{1}{u^2} \left(-f(u)\chi(u)dt^2 + \sum_{i=1}^{3} dx_i^2 + \frac{du^2}{f(u)} \right), \qquad (5.4) $$

the background fields equations of motion are then given as follows

$$ \mathcal{B}_{xy}'' + \mathcal{B}_{xy}' \left[\frac{f'}{f} + \frac{\chi'}{2\chi} - \frac{1}{u} \right] - \frac{\mathcal{B}_{xy}}{u} \left[\frac{f'}{f} + \frac{\chi'}{2\chi} - \frac{1}{u} - \frac{4u^5 Q^2 \gamma \mathcal{B}_{xy}}{f(1 + 4u^2\gamma\mathcal{B}_{xy}^2)^2} + \frac{1}{uf} \right] = 0, \qquad (5.5) $$

$$ f' - \frac{f}{3u} \left[12 + u^2(\mathcal{B}_{xy} - u\mathcal{B}_{xy}')^2 \right] - \frac{1}{3} u\mathcal{B}_{xy}^2 - \frac{u^5 Q^2}{6(1 + 4u^2\gamma\mathcal{B}_{xy}^2)} + \frac{4}{u} = 0, \qquad (5.6) $$

$$ \chi' + \frac{2}{3} u\chi(\mathcal{B}_{xy} - u\mathcal{B}_{xy}')^2 = 0, \qquad (5.7) $$

$$ A_t' + \frac{uQ\sqrt{\chi}}{1 + 4u^2\gamma\mathcal{B}_{xy}^2} = 0. \qquad (5.8) $$
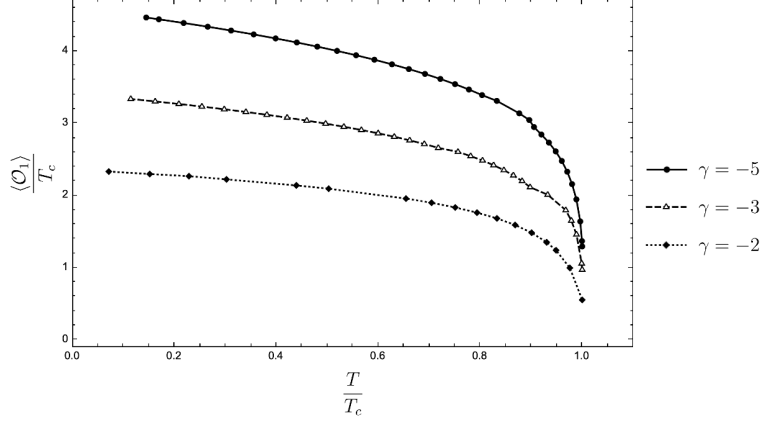
Figure 11. The value of alternative quantization condensate as a function of temperature. From the bottom to the top, various curves correspond to $\gamma = -2, -3$, and -5. The large values of γ give the larger order parameter condensate at $T/T_c = 0$. However, the differential equations turn numerically unstable, causing difficulty in collecting all calculation results in the entire temperature range. So, we have not plotted them here.

where Q is the effective charge density. We utilize the shooting method to search for the solution which satisfies the following boundary conditions,

$$f(u_H), \ A_t(u_H) = 0, \quad \chi(\epsilon) = 1, \quad \mathcal{B}_{xy}(u_H) = \text{finite}, \quad \langle \mathcal{O}_2 \rangle \equiv \mathcal{B}'_{xy}(\epsilon)/2\epsilon = 0, \quad (5.9)$$

to perform the calculation, we consider the near horizon behavior of fields which can be obtained by the Taylor expansion of the fields in the following ways:

$$(\mathcal{B}_{xy}(u), f(u), \chi(u), A_t(u)) \simeq \sum_{i=0}^{n} (b_i, f_i, \chi_i, a_i) \left(1 - \frac{u}{u_H}\right)^i. \quad (5.10)$$

By plugging in the above expansion into the fields equations (5.5)–(5.8), we can determine (b_i, f_i, χ_i, a_i) in terms of the horizon value (b_0, χ_0, u_H). Together with the boundary conditions (5.9) and tuning value of Q, the solutions of the full back-reaction can be obtained.

We examine our calculation by fixing $u_H = 4$, in which the stable solutions can be obtained in various finite values of the coupling constant γ. By tuning $Q \in (0.012, 0.074)$, we get the critical temperature $T_c \approx 0.075$, and the value of the order parameter $\langle \mathcal{O}_1 \rangle$ as a function of temperature, which we found that it is an analogue with holographic superconductor [22]. See figure 11. However, we postpone the physical interests of it for now since our aim in this paper is to show the reliability of our analytic results.

By employing the backreacted background solutions, we can calculate the backreacted fermions spectral function by using flow equation [38]. We divided the temperature regime into three categories: low ($T \ll T_c$), high ($T > T_c$), and medium ($T \sim T_c$) temperature and investigate the spectral function for each regime. In the low-temperature regime, the spectrum is similar to our analytic probe result; this seems natural since, in this regimen, the black-hole temperature is much smaller than the order parameter ($T \ll \langle \mathcal{O}_1 \rangle$). While for $T \sim T_c \sim \langle \mathcal{O}_1 \rangle$, the spectral features remain with fuzzy dressing. Above the T_c, the system is in the normal phase where symmetry is restored, so the spectral function is similar to that of the critical system, which has more fuzziness. See figure 12.
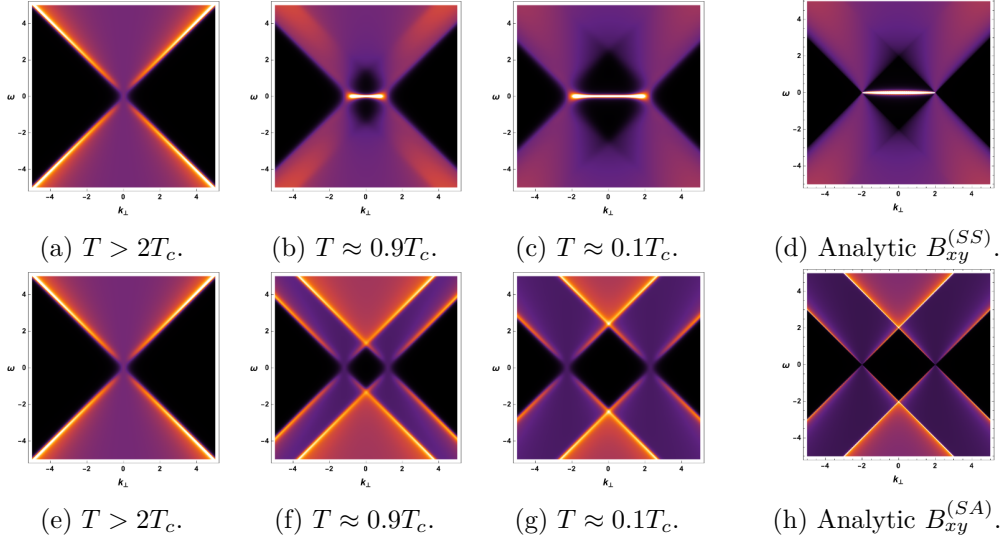
(a) $T > 2T_c$. (b) $T \approx 0.9T_c$. (c) $T \approx 0.1T_c$. (d) Analytic $B_{xy}^{(SS)}$.

(e) $T > 2T_c$. (f) $T \approx 0.9T_c$. (g) $T \approx 0.1T_c$. (h) Analytic $B_{xy}^{(SA)}$.

Figure 12. Backreacted fermions spectral functions (SFs) by fixing the order parameter $\langle \mathcal{O}_1 \rangle \approx 2.0$ at $T \approx 0.1T_c$. (a,e) fermions SF with B_{xy} interaction type at above T_c. In this regime, the symmetry is restored so that $\langle \mathcal{O}_1 \rangle = 0$. (b,f) SFs where the order parameter is of the order of temperature ($T \sim T_c \sim \langle \mathcal{O}_1 \rangle$). (c,g) SFs where the order parameter is much bigger than temperature ($\langle \mathcal{O}_1 \rangle \gg T$). (d,h) SFs generated by our analytic results given in the section 4.

The results reveal the following: i) The degrees of freedom near $\boldsymbol{k}_\perp = |\langle \mathcal{O}_1 \rangle|$ spread out, but the pole singularity structure remains stable. On the other hand, the singularity structure of the branch-cut along $\omega = \pm|(\boldsymbol{k}_\perp \pm \langle \mathcal{O}_1 \rangle)|$ shows deformation. ii) Regardless of fermion quantization, the main spectral functions maintain the same feature as the probe limit results. These results emphasize the reliability of probe-limit results, providing the advantage of avoiding complexities and excessive time calculations associated with full back-reaction calculations.

6 Discussion

In this paper, we found the analytic expressions of the Green's function of fermions under the various types of symmetry breaking: vector and tensor as well as a few types of scalars. We classified the propagator according to the types of singularities: some have branch cut types but some of them have pole types. By having the analytic expressions, although they are within the probe limit, we now understand why various dimensional flat bands exist and why they have finite regions of support.

Our setup refers to the order parameter field configuration with zero sub-leading order term, $\langle \mathcal{O}_\Phi \rangle = 0$. For the scalar condensation in AdS$_4$, an analytic study has already been made and reported [29], but in the context of AdS$_5$, the presence of the condensation term gives the Dirac equations nontrivial dependence of u, making the solvability unavailable for all types of order parameter fields. This is the reason why analytic calculation for condensation was not considered in the present work.

To support the analytic results which are obtained from the probe background and also with only source type order parameters, we performed the numerical analysis to find solutions of a coupled system of gravity with space-like antisymmetric 2-tensor and use it to calculate the spectral function of the fermions. Comparing the spectral functions of fermions with and without the back-reaction, we observed a qualitative agreement in the structural features. In other types of order parameters, we do not show the results in this work, but we also found such qualitative agreement in most cases, which will be extended to future projects.

One should also note that our analytic results are obtained from a pure AdS background. However, we used it to approximate the haired black hole background, not the back reacted near 0 temperature, because in the presence of the order, such zero temperature limit gets a serious modification and becomes a new scaling solution so that it is not for the ordered phase, which is our target. Therefore, our analytic results should be compared with the result at relatively high temperatures where the transition between the strange metal and the ordered state. The singularity structure significantly changes as we change the temperature. The most important remark is that our numerical spectral functions provide slight deformation and a reduction in sharpness compared to analytic results, which is nothing but the effect of the back reaction. However, we observed the different effects of the back reaction on pole and branch-cut type singularity.

In the cases of the pole-type singularity or flat bands, we observe the negligible back reaction and high stability of the flat bands, in which the structure of the singularities qualitatively remains and closely matches our analytic results. Evidently, in the cases where the rotational symmetric flat band is present: $B_{xy}^{(SS)}$, the simple pole singularity structure is remarkably stable. This observation agrees with our previous work, which interpreted the pole spectrum as a topological mode. However, we observed spreading out of the density of state near $\omega = 0, \boldsymbol{k}_\perp = |\langle \mathcal{O}_1 \rangle|$, which is the back-reaction effect.

On the other hand, in the cases of the branch-cut type singularity spectrum, the singularity structure is slightly different from our analytic results. For $B_{xy}^{(SA)}$, we observe that the singularity along $\omega = \pm |(\boldsymbol{k}_\perp \pm \langle \mathcal{O}_1 \rangle)|$ is more fuzzy and reshapes compared to the analytic result. However, it still remains the main feature qualitatively.

We now list a few future projects apart from removing the above limitations. First, discussing the presence of branch-cut singularity in the propagator in view of the non-Fermi Liquid would be interesting. Second, discussing the topology of the various spectral functions should be possible. This would precisely answer the question of what happens to the topology in the limit where the quasi-particle disappears. We hope we can come back to this issue in the near future. Finally, notice that we lack a chiral Γ^5 matrix to represent the chirality of the boundary. For this reason, we did not discuss the chiral dynamics in this paper. We think it must be done by introducing another flavor of fermion to double the degrees of freedom.

Acknowledgments

Interactions	Trace of analytic Green's functions (AdS_4)	Features/Classification
M_0/M_{05}	$\mathrm{Tr}\,\mathbb{G}^{(SA)}_{M_0} \equiv \mathrm{Tr}\,\mathbb{G}^{(SS)}_{M_{50}} = \dfrac{4\omega}{\sqrt{\boldsymbol{k}^2 - \omega^2 + M_0^2}}$	Gapful/s-wave gap
	$\mathrm{Tr}\,\mathbb{G}^{(SS)}_{M_0} \equiv \mathrm{Tr}\,\mathbb{G}^{(SA)}_{M_{50}} = 4\omega\dfrac{\sqrt{\boldsymbol{k}^2 - \omega^2 + M_0^2}}{\boldsymbol{k}^2 - \omega^2 - i\epsilon}$	Topological liquid
B_x/B_{5x}	$\mathrm{Tr}\,G^{(SS)}_{B_x^{(0)}} \equiv \mathrm{Tr}\,G^{(SA)}_{B_{5x}^{(0)}} = \dfrac{2\omega}{\sqrt{(b - k_x)^2 + k_y^2 - \omega^2}} + \dfrac{2\omega}{\sqrt{(b + k_x)^2 + k_y^2 - \omega^2}}$	Shifting cones/p-wave gap
	$\mathrm{Tr}\,\mathbb{G}^{(SA)}_{B_x^{(0)}} \equiv \mathrm{Tr}\,G^{(SS)}_{B_{5x}^{(0)}} = \dfrac{2\omega}{b}\left[\dfrac{(b + k_x)\sqrt{(b - k_x)^2 + k_y^2 - \omega^2} + (b - k_x)\sqrt{(b + k_x)^2 + k_y^2 - \omega^2}}{k_y^2 - \omega^2 - i\epsilon}\right]$	1D flat band
B_{xy}/B_{tu}	$\mathrm{Tr}\,G^{(SA)}_{B_{xy}^{(-1)}} \equiv \mathrm{Tr}\,\mathbb{G}^{(SS)}_{B_{tu}^{(-1)}} = \dfrac{2\omega}{\sqrt{(b - \boldsymbol{k})^2 - \omega^2}} + \dfrac{2\omega}{\sqrt{(b + \boldsymbol{k})^2 - \omega^2}}$	Nodal ring
(anti-symmetric)	$\mathrm{Tr}\,\mathbb{G}^{(SS)}_{B_{xy}^{(-1)}} \equiv \mathrm{Tr}\,\mathbb{G}^{(SA)}_{B_{tu}^{(-1)}} = -\dfrac{2}{b}\left[\dfrac{(b + |\boldsymbol{k}|)\sqrt{(b - \boldsymbol{k})^2 - \omega^2} + (b - |\boldsymbol{k}|)\sqrt{(b + \boldsymbol{k})^2 - \omega^2}}{\omega + i\epsilon}\right]$	2D flat band
B_u	$\mathrm{Tr}\,\mathbb{G}^{(SS)}_{B_u^{(0)}} \equiv \mathrm{Tr}\,\mathbb{G}^{(SA)}_{B_u^{(0)}} = \dfrac{4\omega}{\sqrt{\boldsymbol{k}^2 - \omega^2}}$	QCP
B_{ux}/B_{5u}	$\mathrm{Tr}\,\mathbb{G}^{(SS)}_{B_{ux}^{(-1)}} \equiv \mathrm{Tr}\,\mathbb{G}^{(SA)}_{B_{5u}^{(-1)}} = 4\omega\dfrac{b^2 + \boldsymbol{k}^2 - \omega^2 + f_+ f_-}{f_+ f_-(f_+ + f_-)};\ f_\pm = \sqrt{k_x^2 - \left(b \pm \sqrt{\omega^2 - k_y^2}\right)^2}$	Filled nodal line
	$\mathrm{Tr}\,\mathbb{G}^{(SA)}_{B_{ux}^{(-1)}} \equiv \mathrm{Tr}\,\mathbb{G}^{(SS)}_{B_{5u}^{(-1)}} = 4\omega\dfrac{(f_+ + f_-)\sqrt{\omega^2 - k_y^2} - b(f_+ - f_-)}{\sqrt{\omega^2 - k_y^2}(b^2 + \boldsymbol{k}^2 - \omega^2 + f_+ f_-)};\ f_\pm = \sqrt{k_x^2 - \left(b \pm \sqrt{\omega^2 - k_y^2}\right)^2}$	Non-singular segment
B_t/B_{5t}	$\mathrm{Tr}\,\mathbb{G}^{(SS)}_{B_i^{(0)}} \equiv \mathrm{Tr}\,\mathbb{G}^{(SA)}_{B_{5t}} = 2\left(\dfrac{b + \omega}{\sqrt{\boldsymbol{k}^2 - (b + \omega)^2}} - \dfrac{b - \omega}{\sqrt{\boldsymbol{k}^2 - (b - \omega)^2}}\right)$	Filled nodal ring
	$\mathrm{Tr}\,\mathbb{G}^{(SA)}_{B_i^{(0)}} \equiv \mathrm{Tr}\,\mathbb{G}^{(SS)}_{B_{5t}} = \dfrac{2}{b}\left[\sqrt{\boldsymbol{k}^2 - (b - \omega)^2} - \sqrt{\boldsymbol{k}^2 - (b + \omega)^2}\right]$	Non-singular disk

Table 2. The summary of trace of Green's functions and spectral features in AdS_4. In AdS_4, the Green's functions have duality of the trace part between SS and SA quantization which the key is the fifth gamma matrix Γ^5 which is absent in AdS_5 space-time. It is important to note that $\boldsymbol{k}^2 = k_x^2 + k_y^2$ for all expressions.

A AdS$_4$ Green's function, spectral features, classification, and dualities

Even the spectral functions for AdS_4 were studied in our previous work but the analytic results have not been completely reported yet. However, we found the duality between AdS_4 and AdS_5 Green's functions which we will show in this section. We follow the gamma matrix convention for AdS_4 in [24, 27, 38–40].

$$\Gamma^{\underline{t}} = \sigma_1 \otimes i\sigma_2, \quad \Gamma^{\underline{x}} = \sigma_1 \otimes \sigma_1, \quad \Gamma^{\underline{y}} = \sigma_1 \otimes \sigma_3, \quad \Gamma^{\underline{u}} = \sigma_3 \otimes \sigma_0, \quad \Gamma^5 = i\Gamma^{\underline{t}}\Gamma^{\underline{x}}\Gamma^{\underline{y}}\Gamma^{\underline{u}}. \quad \text{(A.1)}$$

Under this convention, $\Gamma^5 \equiv \Gamma^{\underline{z}}$ in our main AdS_5 context, so that the bulk gamma matrices can be decomposed as follows,

$$\Gamma^{\underline{\mu}} = \begin{pmatrix} 0 & \gamma^{\underline{\mu}} \\ \gamma^{\underline{\mu}} & 0 \end{pmatrix}, \quad \Gamma^{\underline{\mu\nu}} = \begin{pmatrix} \gamma^{\underline{\mu\nu}} & 0 \\ 0 & \gamma^{\underline{\mu\nu}} \end{pmatrix}, \Gamma^{\underline{\mu u}} = \begin{pmatrix} 0 & -\gamma^{\underline{\mu}} \\ \gamma^{\underline{\mu}} & 0 \end{pmatrix},$$

the structure of the gamma matrices shows us that the result of Green's functions will be the same as AdS_5 by removing complex conjugates in the expressions and eliminating

the third momentum k_z. The reason is that the differential equations remain the same as before. For pseudo-interaction types, however, they might be confused due to lack of the fifth gamma matrix in AdS$_5$. According to $\Gamma^5, \Gamma^{5x}, \Gamma^{5t}, \Gamma^{5r}$, they are equivalent to $\Gamma^z, \Gamma^{zx}, \Gamma^{zt}, \Gamma^{zr}$, respectively, by setting $k_z = \mathbf{0}$. As a result, the duality of the Green's functions between AdS$_5$ and AdS$_4$ are obtained. See table 2.

Open Access. This article is distributed under the terms of the Creative Commons Attribution License ([CC-BY4.0](#)), which permits any use, distribution and reproduction in any medium, provided the original author(s) and source are credited.

References

[1] J.M. Maldacena, *The large N limit of superconformal field theories and supergravity*, *Adv. Theor. Math. Phys.* **2** (1998) 231 [`hep-th/9711200`] [ɪɴSPIRE].

[2] E. Witten, *Anti-de Sitter space and holography*, *Adv. Theor. Math. Phys.* **2** (1998) 253 [`hep-th/9802150`] [ɪɴSPIRE].

[3] S.S. Gubser, I.R. Klebanov and A.M. Polyakov, *Gauge theory correlators from noncritical string theory*, *Phys. Lett. B* **428** (1998) 105 [`hep-th/9802109`] [ɪɴSPIRE].

[4] E. Alvarez and C. Gomez, *Geometric holography, the renormalization group and the c theorem*, *Nucl. Phys. B* **541** (1999) 441 [`hep-th/9807226`] [ɪɴSPIRE].

[5] V. Balasubramanian and P. Kraus, *Space-time and the holographic renormalization group*, *Phys. Rev. Lett.* **83** (1999) 3605 [`hep-th/9903190`] [ɪɴSPIRE].

[6] J. de Boer, E.P. Verlinde and H.L. Verlinde, *On the holographic renormalization group*, *JHEP* **08** (2000) 003 [`hep-th/9912012`] [ɪɴSPIRE].

[7] S.A. Hartnoll, A. Lucas and S. Sachdev, *Holographic quantum matter*, MIT Press, Cambridge, MA, U.S.A. (2018).

[8] J. Zaanen, Y.-W. Sun, Y. Liu and K. Schalm, *Holographic duality in condensed matter physics*, Cambridge University Press, Cambridge, U.K. (2015) [`DOI:10.1017/CBO9781139942492`] [ɪɴSPIRE].

[9] S. Sachdev, *Quantum phase transitions*, second edition, Cambridge University Press, Cambridge, U.K. (2011).

[10] K.G. Wilson, *Renormalization group and critical phenomena. 1. Renormalization group and the Kadanoff scaling picture*, *Phys. Rev. B* **4** (1971) 3174 [ɪɴSPIRE].

[11] K.G. Wilson, *The renormalization group: critical phenomena and the Kondo problem*, *Rev. Mod. Phys.* **47** (1975) 773 [ɪɴSPIRE].

[12] P. Kovtun, D.T. Son and A.O. Starinets, *Viscosity in strongly interacting quantum field theories from black hole physics*, *Phys. Rev. Lett.* **94** (2005) 111601 [`hep-th/0405231`] [ɪɴSPIRE].

[13] J. Crossno et al., *Observation of the Dirac fluid and the breakdown of the Wiedemann-Franz law in graphene*, *Science* **351** (2016) aad0343 [ɪɴSPIRE].

[14] A. Lucas et al., *Transport in inhomogeneous quantum critical fluids and in the Dirac fluid in graphene*, *Phys. Rev. B* **93** (2016) 075426 [`arXiv:1510.01738`] [ɪɴSPIRE].

[15] Y. Seo et al., *Holography of the Dirac fluid in Graphene with two currents*, *Phys. Rev. Lett.* **118** (2017) 036601 [`arXiv:1609.03582`] [ɪɴSPIRE].

[16] Y. Seo, G. Song and S.-J. Sin, *Strong correlation effects on surfaces of topological insulators via holography*, *Phys. Rev. B* **96** (2017) 041104 [arXiv:1703.07361] [ɪɴSPIRE].

[17] Y. Seo, G. Song, C. Park and S.-J. Sin, *Small Fermi surfaces and strong correlation effects in Dirac materials with holography*, *JHEP* **10** (2017) 204 [arXiv:1708.02257] [ɪɴSPIRE].

[18] M. Liu et al., *Crossover between weak antilocalization and weak localization in a magnetically doped topological insulator*, *Phys. Rev. Lett.* **108** (2012) 036805.

[19] D. Zhang et al., *Interplay between ferromagnetism, surface states, and quantum corrections in a magnetically doped topological insulator*, *Phys. Rev. B* **86** (2012) 205127.

[20] S.H. Shenker and D. Stanford, *Stringy effects in scrambling*, *JHEP* **05** (2015) 132 [arXiv:1412.6087] [ɪɴSPIRE].

[21] N. Lashkari et al., *Towards the fast scrambling conjecture*, *JHEP* **04** (2013) 022 [arXiv:1111.6580] [ɪɴSPIRE].

[22] S.A. Hartnoll, C.P. Herzog and G.T. Horowitz, *Holographic superconductors*, *JHEP* **12** (2008) 015 [arXiv:0810.1563] [ɪɴSPIRE].

[23] S.S. Gubser, *Breaking an Abelian gauge symmetry near a black hole horizon*, *Phys. Rev. D* **78** (2008) 065034 [arXiv:0801.2977] [ɪɴSPIRE].

[24] E. Oh, Y. Seo, T. Yuk and S.-J. Sin, *Ginzberg-Landau-Wilson theory for flat band, Fermi-arc and surface states of strongly correlated systems*, *JHEP* **01** (2021) 053 [arXiv:2007.12188] [ɪɴSPIRE].

[25] S.-S. Lee, *A non-Fermi liquid from a charged black hole: a critical Fermi ball*, *Phys. Rev. D* **79** (2009) 086006 [arXiv:0809.3402] [ɪɴSPIRE].

[26] M. Cubrovic, J. Zaanen and K. Schalm, *String theory, quantum phase transitions and the emergent Fermi-liquid*, *Science* **325** (2009) 439 [arXiv:0904.1993] [ɪɴSPIRE].

[27] H. Liu, J. McGreevy and D. Vegh, *Non-Fermi liquids from holography*, *Phys. Rev. D* **83** (2011) 065029 [arXiv:0903.2477] [ɪɴSPIRE].

[28] N. Iqbal and H. Liu, *Real-time response in AdS/CFT with application to spinors*, *Fortsch. Phys.* **57** (2009) 367 [arXiv:0903.2596] [ɪɴSPIRE].

[29] E. Oh, T. Yuk and S.-J. Sin, *The emergence of strange metal and topological liquid near quantum critical point in a solvable model*, *JHEP* **11** (2021) 207 [arXiv:2103.08166] [ɪɴSPIRE].

[30] H. Im et al., *Observation of Kondo condensation in a degenerately doped silicon metal*, *Nature Phys.* **19** (2023) 676 [arXiv:2301.09047] [ɪɴSPIRE].

[31] T. Faulkner and J. Polchinski, *Semi-holographic Fermi liquids*, *JHEP* **06** (2011) 012 [arXiv:1001.5049] [ɪɴSPIRE].

[32] N. Iqbal, H. Liu and M. Mezei, *Quantum phase transitions in semilocal quantum liquids*, *Phys. Rev. D* **91** (2015) 025024 [arXiv:1108.0425] [ɪɴSPIRE].

[33] K. Jensen, *Semi-holographic quantum criticality*, *Phys. Rev. Lett.* **107** (2011) 231601 [arXiv:1108.0421] [ɪɴSPIRE].

[34] G.T. Horowitz and M.M. Roberts, *Zero temperature limit of holographic superconductors*, *JHEP* **11** (2009) 015 [arXiv:0908.3677] [ɪɴSPIRE].

[35] J.-W. Chen et al., *Towards a holographic model of D-wave superconductors*, *Phys. Rev. D* **81** (2010) 106008 [arXiv:1003.2991] [ɪɴSPIRE].

[36] F. Benini, C.P. Herzog and A. Yarom, *Holographic Fermi arcs and a d-wave gap*, *Phys. Lett. B* **701** (2011) 626 [`arXiv:1006.0731`] [ɪɴSPIRE].

[37] D. Ghorai, T. Yuk and S.-J. Sin, *Order parameter and spectral function in d-wave holographic superconductors*, *Phys. Rev. D* **109** (2024) 066004 [`arXiv:2309.01634`] [ɪɴSPIRE].

[38] T. Yuk and S.-J. Sin, *Flow equation and fermion gap in the holographic superconductors*, *JHEP* **02** (2023) 121 [`arXiv:2208.03132`] [ɪɴSPIRE].

[39] Y.-K. Han, J.-W. Seo, T. Yuk and S.-J. Sin, *Holographic Lieb lattice and gapping its Dirac band*, *JHEP* **02** (2023) 084 [`arXiv:2205.12540`] [ɪɴSPIRE].

[40] J.-W. Seo, T. Yuk, Y.-K. Han and S.-J. Sin, *ABC-stacked multilayer graphene in holography*, *JHEP* **11** (2022) 017 [`arXiv:2208.14642`] [ɪɴSPIRE].

[41] R.-G. Cai and R.-Q. Yang, *Antisymmetric tensor field and spontaneous magnetization in holographic duality*, *Phys. Rev. D* **92** (2015) 046001 [`arXiv:1504.00855`] [ɪɴSPIRE].

[42] B. Altschul, Q.G. Bailey and V.A. Kostelecky, *Lorentz violation with an antisymmetric tensor*, *Phys. Rev. D* **81** (2010) 065028 [`arXiv:0912.4852`] [ɪɴSPIRE].